Supporting Information

69451 Weinheim, Germany

A General Strategy to Control Viscosity Sensitivity of Molecular Rotor-Based Fluorophores

Songtao Ye [a], Han Zhang [a], Jinyu Fei [a], Charles H. Wolstenholme [a] and Xin Zhang*[a,b]

[a]Department of Chemistry, [b]Department of Biochemistry and Molecular Biology, Pennsylvania State University, University Park, PA 16802, USA

SUPPORTING INFORMATION

Table of Contents

SUPPORTING INFORMATION

1. Experimental Procedures

1.1 Absorbance spectra.

Absorbance spectra were collected using an Agilent Cary 300 UV/Vis spectrometer. Fluorophores were prepared with final concentration of 10 μM in glycerol at room temperature and transferred in a quartz cuvette for measurements.

1.2 Fluorescence excitation and emission spectra.

Fluorescence excitation and emission spectra were recorded using a Tecan infinite M1000Pro fluorescence microplate reader. For both spectra, fluorophores were prepared at 10 μM in glycerol at room temperature and 150 μL of each sample was transferred into a Costar® black polystyrene 96-well plate for measurements. Each spectrum was normalized against its maxima to give the finalized spectra.

1.3 Quantum yield and molar extinction coefficient.

Quantum yield was measured according to a published guideline[1]. In brief, fluorophores were diluted from 2 mM DMSO stock solution into a desired solvent with 2, 4, 6, 8, 10 μM as the final concentration. For each individual concentration, absorbance and emission spectrum was collected. The integration of emission spectrum was then plotted against the absorbance value at the excitation wavelength. The slope of the regression line was used to calculate the quantum yield by comparing against a reference fluorophore (Rhodamine 110, ϕ = 0.88 in EtOH; Coumarin 6, ϕ = 0.82 in EtOH; Cy®3, ϕ = 0.15 in H_2O) according to the following equation:

$$\phi_x = \phi_{ref}\left(\frac{Gradient_x}{Gradient_{Ref}}\right)\left(\frac{n_x^2}{n_{ref}^2}\right)$$

Where the ϕ is the quantum yield, n is the refractive index of the solvent and subscripts x and ref stand for fluorophore-of-interest and reference fluorophore, respectively. Molar extinction coefficient was determined as the slope of the linear correlation by plotting absorbance maxima against concentration of the fluorophore.

1.4 Viscosity sensitivity measurements.

Viscosity sensitivity was measured according to a published protocol[2]. Fluorophores are diluted from 2 mM DMSO stock into a series of ethylene glycol and glycerol mixture at 20 ˚C with a final concentration 10 μM. The composition and viscosity of each mixture at 20 ˚C is described in Table S1. 100 μL of sample from each mixture was then transferred into a Costar® black polystyrene 96-well plate to collect the emission spectrum. Emission peak intensity was plotted as a function of solvent viscosity in a double logarithm manner and fitted by linear regression. The slope of the regression line represents the viscosity sensitivity value.

1.5 Mechanistic study of rotational energy barrier E_a.

Emission spectrum for fluorophores were recorded in methanol and glycerol mixtures at 22.0˚C, 37.0˚C and 42˚C using a Tecan infinite M1000Pro fluorescence microplate reader with temperature control function. Emission spectrum for fluorophores at 4.0˚C were recorded using same instrument by incubating a preloaded 96-well plate in 4.0˚C fridge overnight. All fluorophores were dissolved with a final concentration at 10 μM and excited at a wavelength that corresponds to their absorption peak. A series of water and glycerol mixture with final mass percentage 30%, 40%, 50%, 60%, 70%, 80% and 90% of glycerol were used in this experiment. The viscosities of the mixture were estimated based on water-glycerol mixture at above mentioned temperature based on a published paper[3].

1.6 Plasmid construction.

SOD1(A4V)-Halo-His6 was constructed from on a previously established construct[4] SOD1(WT)-Halo-His6 from our lab. The A4V mutation was introduced to SOD1 via Quickchange PCR. Fluc(R188Q) was acquired as a generous gift from Ulric Hartl (Addgene Plasmid # 90171). This gene was sub-cloned into a pET29b vector containing Halo-6His by PIPE cloning method to generate Fluc(R188Q)-Halo-His6. Other plasmids used in the work, including E. coli expression vectors encoding HaloTag-His6 and α-synuclein, mammalian expression vectors encoding Htt-46Q-Halo and Htt-110Q-Halo were constructed according to our previously published work[4-5].

1.7 Protein expression and purification.

For SOD1(A4V)-Halo-6His and Fluc(R188Q)-Halo-6His, plasmids were transformed into E. coli BL21 DE3* harboring a pBAD vector encoding σ32-I54N, respectively. Single colony was picked up and inoculated into 5 mL LB (Dot Scientific) containing ampicillin and kanamycin, followed by serial dilution with 10^4 and 10^6. The cultures were allowed to grow overnight at 37˚C with shaking at 210 rpm. When OD_{600} reached 0.8-1.0 (either 10^4 or 10^6 dilution, whichever reached first), 15 mL of starting culture was introduced into a culture flask containing 1.5 L LB media with ampicillin and kanamycin. 3 g l-arabinose (a final concentration of 0.2 mg/ml) was added when OD_{600} reached 0.3-0.4, followed by adding 750 μL 1 M isopropyl β-D-1-thiogalactopyranoside (a final concentration of 0.5 mM) when OD_{600} reached 0.7-0.8 to induce the expression of recombinant protein. Cultures were allowed to shake overnight at 18 ˚C, harvested and stored in -80˚C freezer until use. To carry out protein purification, cells were thawed and lysed by sonication on ice in buffer A (50 mM Tris-HCl, pH 7.5, 100 mM NaCl) in the presence of 1 mM phenylmethyl sulfonyl fluoride (PMSF). The lysate was cleared out by centrifuging at 16,000 g for 60 min at 4˚C. Supernatant was collected and loaded onto a 6 mL pre-charged IMAC column (Profinity™ IMAC Resin, Bio-Rad), followed by a washing step with buffer A. SOD1 or Fluc was then eluted with gradient addition of buffer B (50 mM Tris-HCl, pH 7.5, 100 mM NaCl, 500 mM imidazole) over 8 CV. The fraction was collected, pooled and loaded onto a gel filtration column (HiPrep™ 16/60 Sephacryl™ S200HR, GE Healthcare) to allow further purification and buffer exchange (50 mM Tris-HCl, pH

7.5, 100 mM NaCl). The resulted protein fractions were analyzed by SDS-PAGE to have >95% purity before concentrated and flash freeze. Halo-6His and a-synuclein purification could be found elsewhere[4].

1.8 In Vitro protein aggregation assay.

SOD1(A4V)-Halo: 42 μM SOD1 was labeled with 5 μM **P1a** or **P1b** for 10 min on ice in stock solution (50 mM Tris-HCl, pH 7.5, 100 mM NaCl) to allow bio-orthogonal conjugation. 80 mM EDTA was added after 10-min incubation to chelate the structural metal of SOD1, followed by aliquoting the stock solution into ten 1.5 mL Eppendorf tubes. The tubes were put into a 59˚C heat block to initiate aggregation. Each tube was taken out at a given timepoint (0, 1, 2.5, 5, 7.5, 10, 12.5, 15, 17.5 and 20 minutes) to measure the fluorescence using a Tecan infinite M1000Pro fluorescence microplate reader. Fluorescence of **P1a** and **P1b** were measured at Ex = 530 nm/Em = 600 nm and Ex = 595 nm/Em = 714 nm, respectively.

Fluc(R188Q)-Halo: A similar procedure as SOD1 was conducted to carry out aggregation of firefly luciferase. Addition of EDTA is omitted and the heat block was pre-set to 57 ˚C to initiate aggregation.

α-synuclein: Aggregation assay was conducted in accordance with a previously published protocol[4]. In brief, 10 μM **ThT**, **1a** and **1b** was added to 140 μM a-synuclein (buffer condition: 20 mM HEPES, pH 7.5, 100 mM NaCl), respectively. 150 μL protein-dye mixture was loaded into a clear bottom 96 well plate, followed by sealing with Mylar sealer. Aggregation was at 37˚C with shaking at 1,350 rpm. The plate was taken out at each timepoint to measure the fluorescence using a Tecan infinite M1000Pro fluorescence microplate reader. Fluorescence intensities were measured at Ex = 450 nm/Em = 480 nm for **ThT**, Ex = 530 nm/Em = 600 nm for **1a** and Ex = 595 nm/Em = 714 nm for **1b**.

1.9 Live cell imaging.

HEK293T cells were seeded at ~15% confluency in 35 mm glass bottom dish (poly-D-lysine treated, MetTek Corporation) in Dulbecco's modified Eagle's medium (DMEM, Gibco) supplemented with 10% Fetal Bovine Serum (FBS, Gibco) and 0.5 % mg/mL penicillin-streptomycin-glutamine (PSQ, Gibco). When cells reached 40% confluency, replace 50% of the old DMEM media with fresh DMEM containing 1 μM **P2a** and **P2b**, hence reaching 0.5 μM as the final concentration. Mammalian expression Htt-46Q-Halo or Htt-110Q-Halo were transiently transfected in to HEK293T cells and expressed for 48 h. After 48 h, excess probes were washed away by replacing the old DMEM media with fresh media containing 0.1 μg/mL Hoechst 33342 at 30 min prior to confocal microscopy experiments. Live cell imaging was carried out using Olympus FV1000 confocal microscope. Hoechst 33342, **P2a** and **P2b** were excited using 405 nm, 458 nm and 543 nm lasers respectively. Results were analyzed using software Fiji.

1.10 General synthetic and chromatographic methods.

All reagents are commercial grade unless otherwise stated. Reactions were carried out in Synthware® round bottom flask and monitored via thin layer chromatography (Silicycle®, 60 Å). Products were purified using either Agilent 1260 Infinity High Performance Liquid Chromatography (equipped with reverse phase C18 column) or flash column chromatography (Silica Flash® F60). ^{1}H NMR and ^{13}C NMR were performed on a Bruker AV-III-HD-500 spectrometer or Bruker AVANCE^{TM} 400 spectrometer in d_6-dimethylsulfoxide or Chloroform-d from Cambridge Isotope Laboratories. Chemical shifts were referenced to tetramethylsilane (TMS) standard. High resolution mass spectra were obtained on a Waters Q-TOF quadrupole/time-of-flight spectrometer.

2. Supplementary Notes

Note S1. RBFs bear distinct *x* exhibit best resolution in different viscosity regions.

It is vital for the application of RBFs that large fluorescence intensity change could be introduced by small viscosity change, hence better resolution and reduced errors. Despite the Föster-Hoffmann equation describes the relationship between the quantum yield ∅ and viscosity η, it does not provide a straightforward impression as how RBFs fluoresce in different viscosity since both ∅ and η are in logarithmic scale. Using mathematical calculation, it is indisputable that fluorophores with high viscosity sensitivity *x* would achieve higher fluorescence fold-of-change across all viscosity regions. However, when compare the resolution and errors of RBFs, fluorescence fold-of-change become ill-suited, particularly when fluorophores are dark. Instead, the absolute fluorescence increase would be more relevant. As demonstrated below, fluorophores with low viscosity sensitivity *x* showed best resolution when detecting small viscosity changes in low viscosity region, whereas fluorophores with high *x* are suited to detect large viscosity changes to an end point with a high viscosity.

We directly compared the fluorescence quantum yield (∅) of the benzothiazole scaffold RBFs, **ThT**, **1a** and **1b**. The quantum yield was calculated using Föster-Hoffmann equation over a wide range of viscosity (1-1000 mPa·s) and summarized in **Table S4**. The ∅ value was normalized against ∅ measured in 1000 mPa·s to give a percentage change ∅, here in named as ∅%. Then, we analyzed the ∅% increase and the actual ∅ value of **ThT**, **1a** and **1b,** with the hope to find the viscosity region that RBFs give the greatest increase of ∅% and a reasonable ∅ values for imaging applications.

As shown in **Table S4**, **ThT** indeed showed the greatest extent of fluorescence activation (250-fold) when viscosity changes from 1 to 1,000 mPa·s. Whereas, probes **1a** and **1b** increased their fluorescence quantum yield by more modest fold-of-change as 33-fold and 9-fold, respectively. Thus, the intrinsically high *x* value of **ThT** makes it the most suited probe for detecting large increase of viscosity, such as changes from folded proteins to insoluble aggregates.

However, probes **1a** and **1b** are more suited to detect small changes of viscosity as shown below. We analyzed small viscosity changes at a low viscosity region (1-200 mPa·s). In this region, despite **ThT** (*x* = 0.79) showed a significant fluorescence fold-of-change (from 0.4% to 28%, 70-fold), ∅ values remained relatively low (from ~0.00 to 0.04). By contrast, probes **1a** (*x* = 0.51) exhibited a 11-fold fluorescence increase to a 44% ∅% in the same viscosity region, resulting in ∅ value of 0.35. Similarly, probes **1b** (*x* = 0.32) showed a 5-fold fluorescence increase, resulting in a 60% ∅% and ∅ value of 0.31. Thus, although **ThT** did most significantly increased its fluorescence by 70-fold, the very low quantum yield at the region of 1-200 mPa·s (from ~0.00 to 0.04) makes it unsuitable detect changes of viscosity in this region. By contrast, probes **1a** and **1b** are suited probes to detect small changes in the low viscosity regions, such as misfolding of folded proteins to form misfolded oligomers.

In addition, we further measured the fluorescence response of **ThT**, **1a** and **1b** focusing on small viscosity regions (0-100 mPa·s) as shown in **Figure S8**. In this experiment, 5 μM probes were incubated in water-glycerol mixture with varying viscosity (1, 5 10, 20, 50 and 100 mPa·s). The emission spectra were acquired and averaged over 3 independent measurements (standard error, n =3). We found that all three fluorophores showed discernable fluorescence increase as low as 4 mPa·s (from 1 to 5 mPa·s). More importantly, **1b** exhibited the largest fluorescence intensity gain at low viscosity, which is in agreement data presented in **Table S4**.

Thus, given that the *x* values decrease in the sequence of **ThT**, **1a** and **1b**, this result support the notion that fluorophores with low viscosity sensitivity *x* showed best resolution in low viscosity region, whereas fluorophores with high *x* are suited for high viscosity.

3. Supplementary Figures and Tables

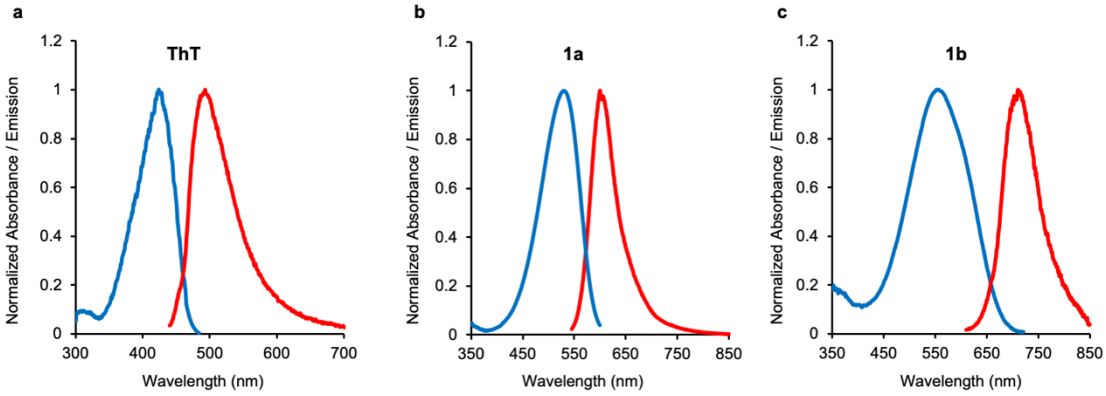

Figure S1. Normalized absorption and emission spectra of **ThT**, **1a** and **1b** in glycerol.

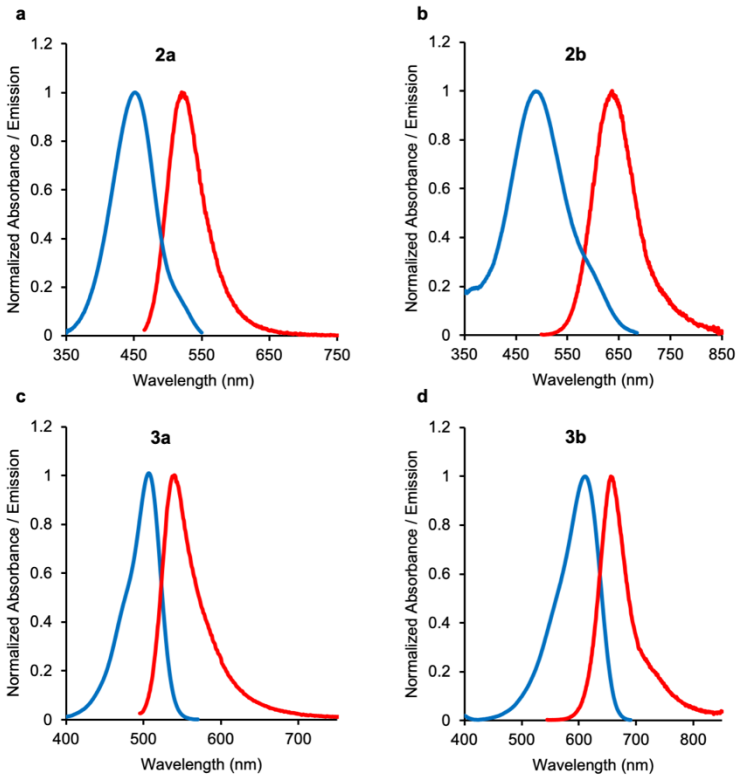

Figure S2. Normalized absorption and emission spectra of **2a**, **2b, 3a** and **3b** in glycerol.

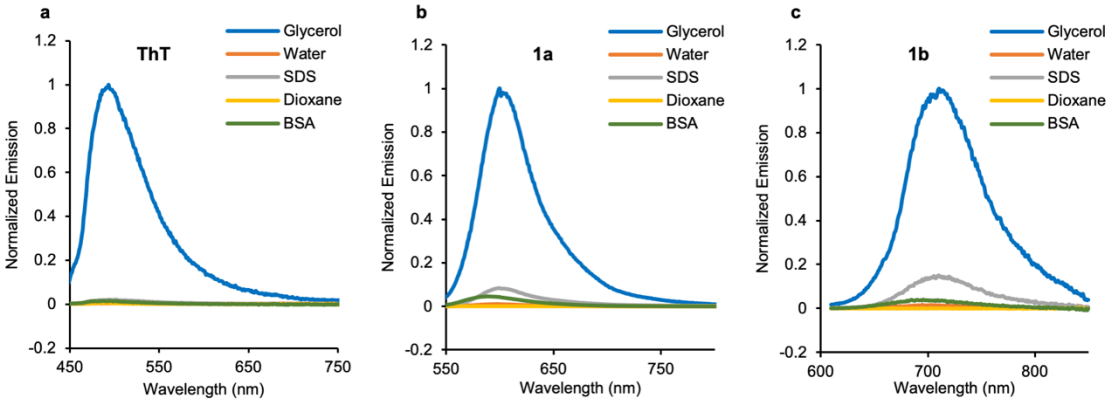

Figure S3. Fluorescence emission spectra of **ThT, 1a** and **1b** to glycerol, water, SDS, 1,4-dioxane and BSA**.** 10 μM of fluorophore was incubated in glycerol, water, SDS (0.2%), BSA (2 mg/mL), and dioxane. Intensities were normalized against the value in glycerol. (**a-c**) **ThT**, **1a** and **1b** were excited at 427nm, 530 nm and 595 nm, respectively.

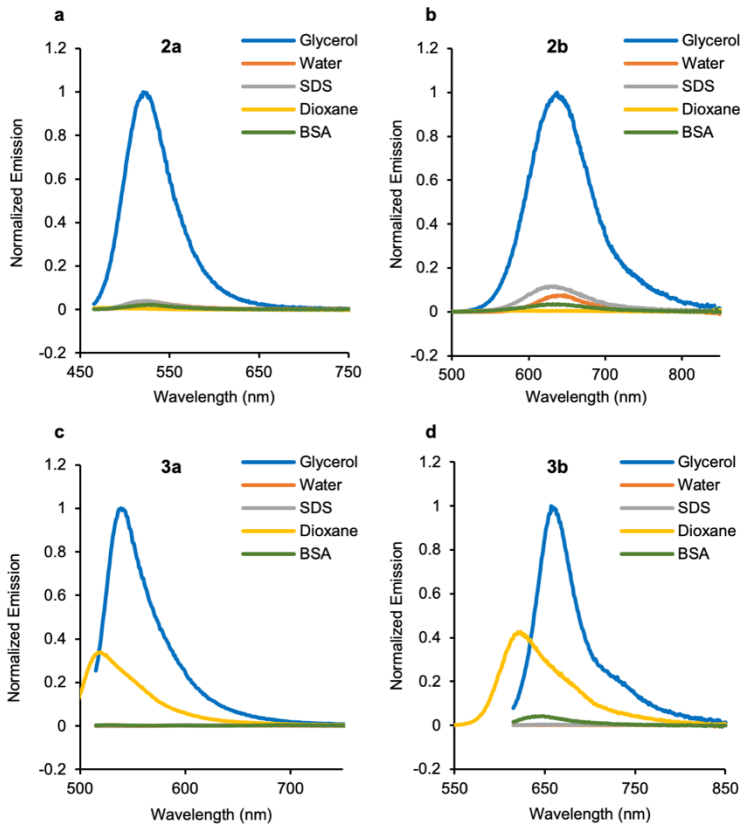

Figure S4. Fluorescence emission spectra of **2a, 2b, 3a** and **3b** to glycerol, water, SDS, 1,4-dioxane and BSA**.** 10 μM of fluorophore was incubated in glycerol, water, SDS (0.2%), BSA (2 mg/mL), and dioxane. Intensities were normalized against the value in glycerol. (**a**-**b**) **2a** and **2b** were excited at 450 nm and 485 nm, respectively. (**c**-**d**) For samples in glycerol, water, SDS and BSA solution, **3a** and **3b** were excited at 500 nm and 600 nm, respectively. Because DCDHF (**3a** and **3b**) is known to be a class of solvatochromic fluorophores, thus **3a** and **3b** were excited at 485 nm and 531 nm in 1,4-dioxane, respectively.

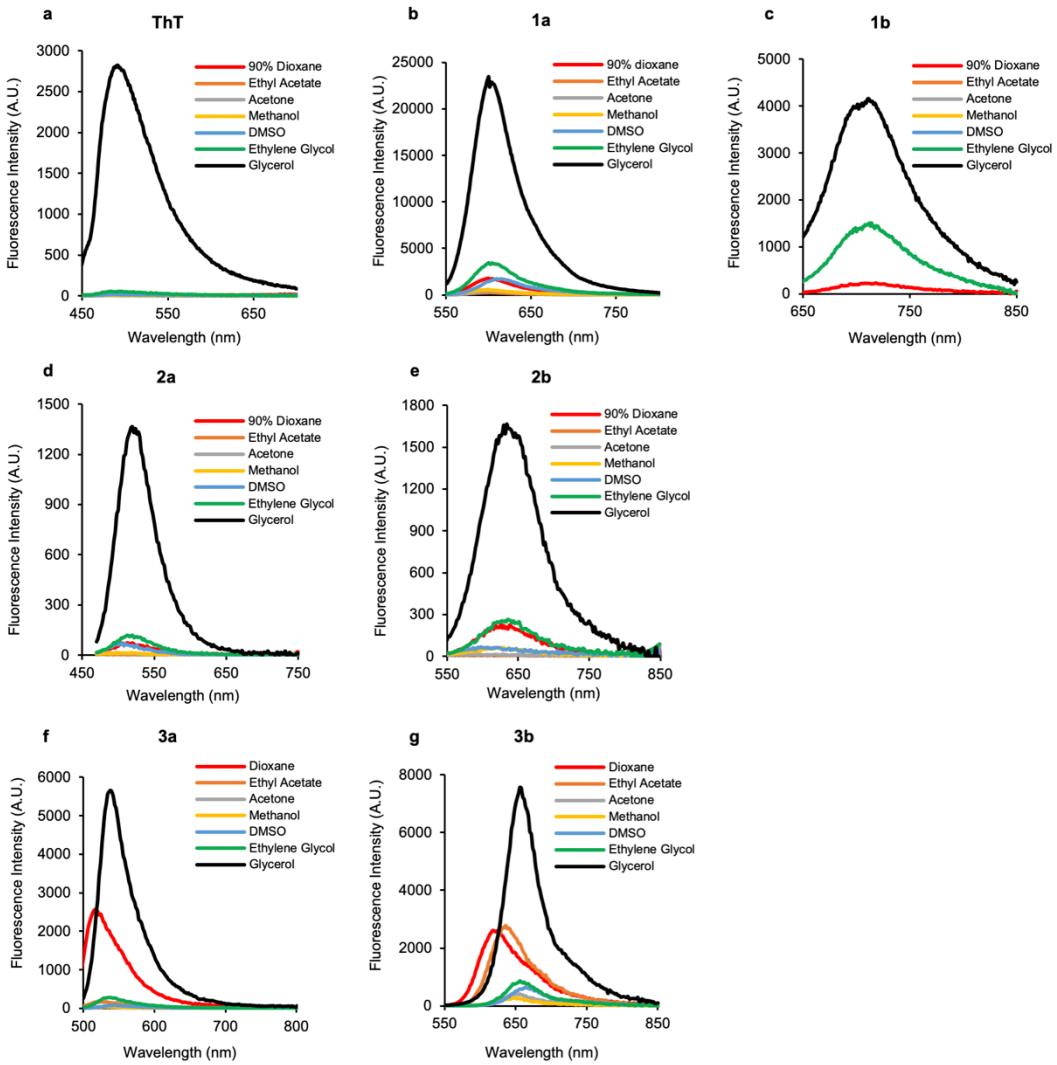

Figure S5. Fluorescence emission spectra of fluorophores in organic solvents with different polarity. 5 μM of fluorophores were incubated in dioxane (or 90 vol% dioxane in water to avoid aggregation caused quenching), ethyl acetate, acetone, methanol and dimethyl sulfoxide, the emission spectra were collected and compared to ethylene glycol and glycerol which are known for enhanced viscosity. (**a-c**) **ThT**, **1a** and **1b** were excited at 420 nm, 530 nm and 600 nm, respectively. (**d-e**) **2a** and **2b** were excited at 450 nm and 485 nm, respectively. The fluorescence turn-on for benzothiazolium class and HBI class dyes is predominantly coming from enhanced viscosity but not reduced polarity. (**f-g**) **3a** and **3b** were excited at 470 nm and 530 nm, respectively. DCDHF is known to be solvatochromic and viscosity sensitive. Their fluorescence turn-on can be triggered by both reduced polarity and enhanced polarity. Significant hypsochromic shifts were also observed for **3a** and **3b** in solvent with reduced polarity, defined by their solvatochromic nature.

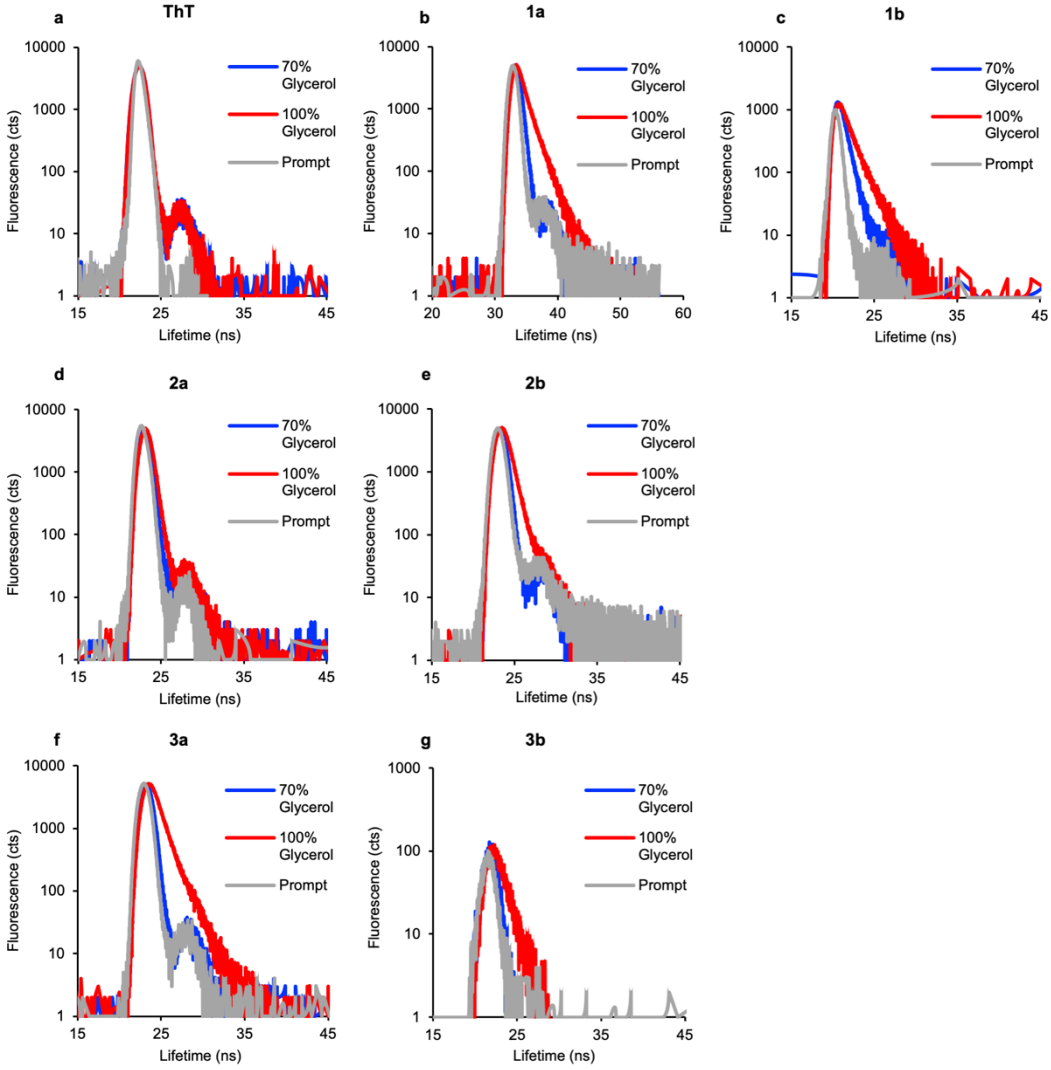

Figure S6. Time-resolved fluorescence decay of reported probes in solvents with low viscosity (70 vol% glycerol in water, 30 mPa·s) and high viscosity (100% glycerol, 1078 mPa·s) at 23˚C [3]. Samples were prepared at a 5 μM concentration in desired solution. Time correlated single photon counting data were generated using a Horiba FluoroMax-4 spectrofluorometer equipped with Horiba NanoLED pulsed light source (455nm, 495 nm and 560 nm). Single and double exponential fitting were performed to generate the lifetime of fluorophores in this work, summarized in Table S4.

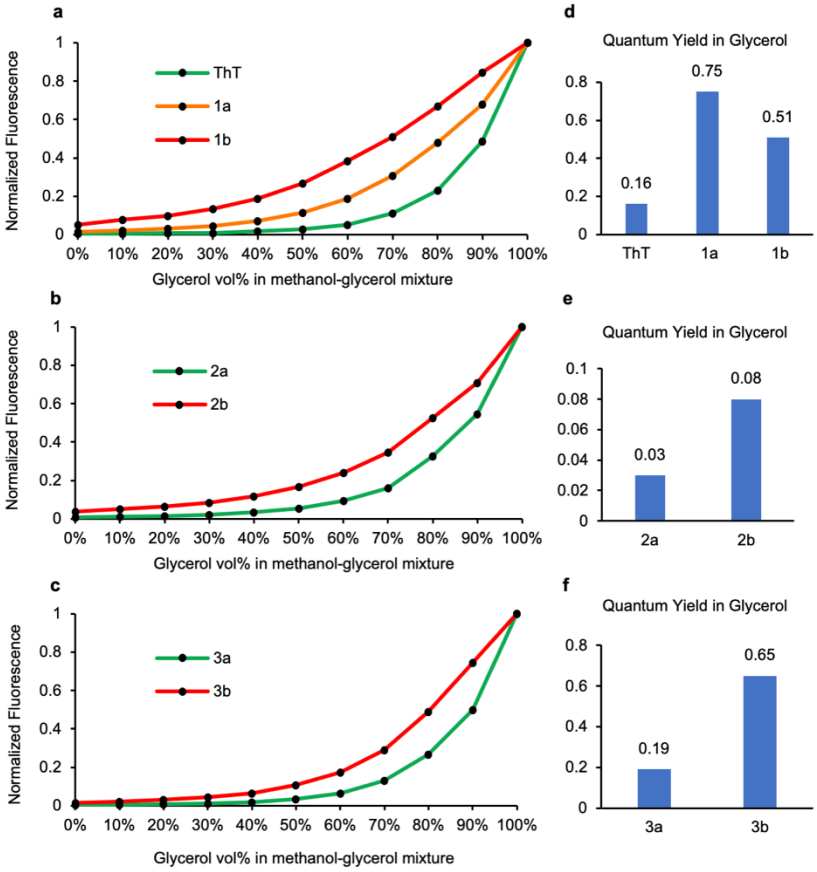

Figure S7. (**a-c**) Fluorescence intensities for RBFs (10 μM) measured in methanol-glycerol gradient. (**d-f**) Quantum yield of RBFs (10 μM) measured in 100% glycerol at room temperature, which correspond to the end points of the measurement in **a-c**.

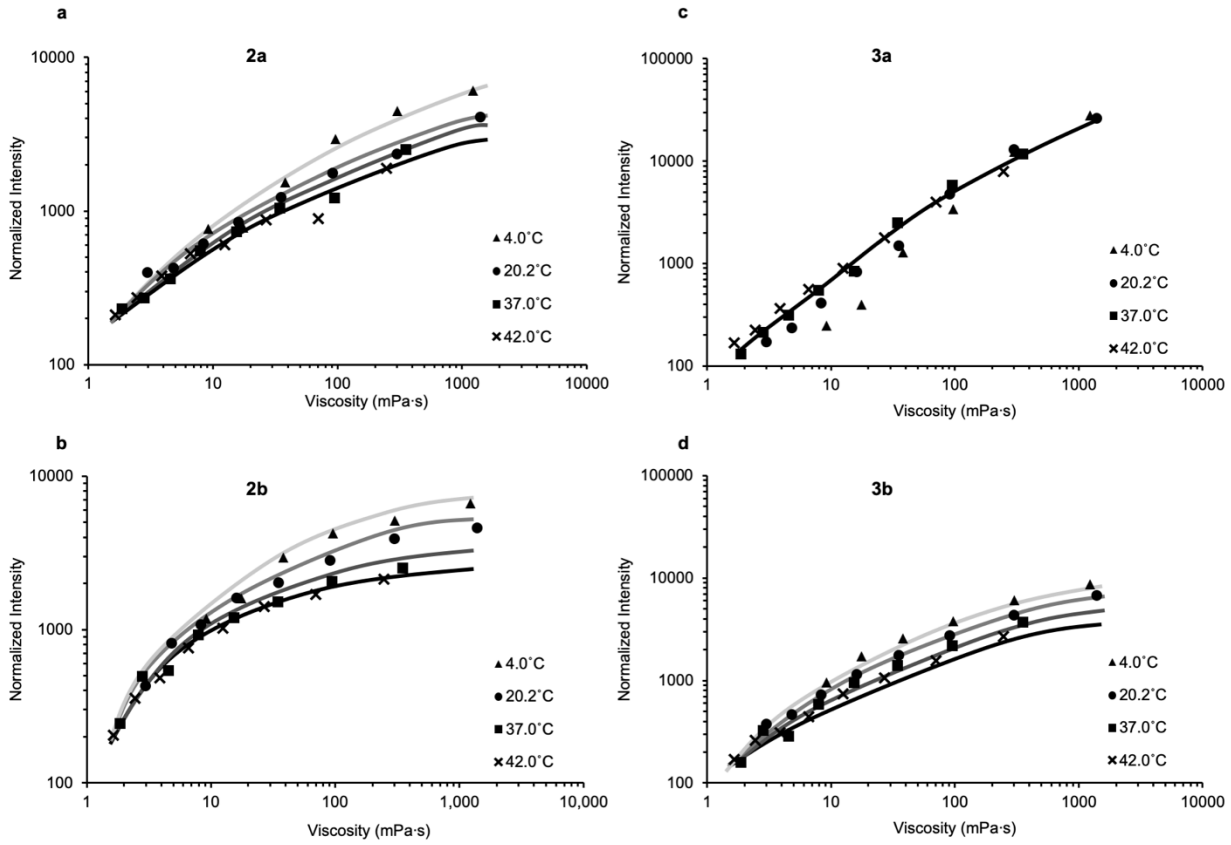

Figure S8. Fluorescence intensities for RBFs (10 μM) measured in methanol-glycerol gradient at different temperature. The discrepancies between each curve represents the relative rotational energy barrier E_a: with a higher E_a, we expect a great difference of fluorescence intensities when varying temperatures at high viscosity. (**a-b**) Fluorescence intensity of **2a** and **2b**, wherein **2a** showed a smaller fluorescence intensity discrepancy (notably at 20.2˚C, 37.0˚C and 42.0˚C) compared to **2b**, indicating that the E_a height of **2a** is smaller than **2b**. (**c-d**) Fluorescence intensity of **3a** and **3b**, wherein fluorescence of **3a** at all temperatures remained largely unchanged, indicating a low E_a height. Whereas, **3b** exhibited a great temperature difference in conditions with high viscosity, indicating a higher E_a.

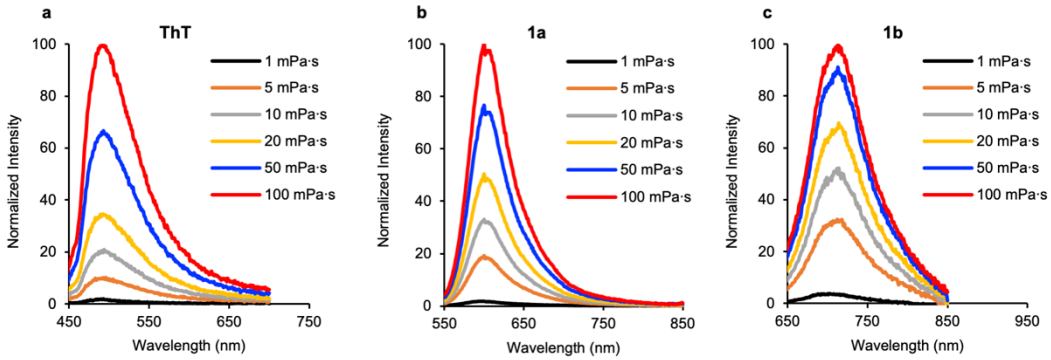

Figure S9. Normalized fluorescence emission spectrum of **ThT**, **1a** and **1b** in water-glycerol mixture with varying viscosity (1, 5 10, 20, 50 and 100 mPa·s). 5 μM of **ThT**, **1a** and **1b** were excited at 420nm, 530 nm and 595 nm, respectively. Data were obtained using a Tecan infinite M1000Pro fluorescence microplate reader and averaged over 3 independent measurements (standard error, n = 3). The emission curve showed discernable separation across the entire viscosity range with smallest intervals as low as 4 mPa·s. It is important to note that the fluorogenic response of RBFs is not evenly distributed across the entire viscosity range, hence the resolution varies (see Note S1). Viscosities were derived based on a published protocol [3].

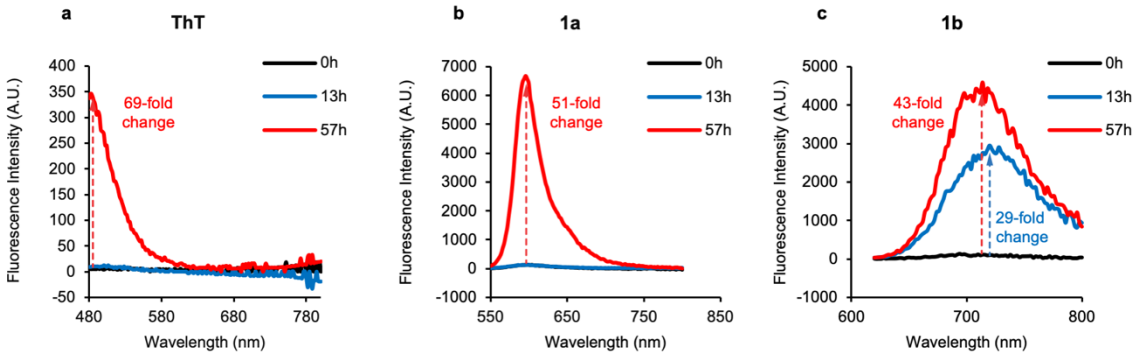

Figure S10. Fluorescence intensity increase of **ThT**, **1a** and **1b** at 13 h (soluble oligomers) and 57 h (mature fibers) during *a*-synuclein aggregation. (**a-b**) 69-fold and 51-fold fluorescence intensity increases were observed after 57 h of incubation for **ThT** (x = 0.79) and **1a** (x = 0.51), respectively. No significant fluorescence turn-on was found after 13 h of incubation. (**c**) **1b** (x = 0.32) exhibited a 29-fold fluorescence intensity increase after 13 h of incubation, and its fluorescence intensity further increased to 43-fold after 57h of incubation.

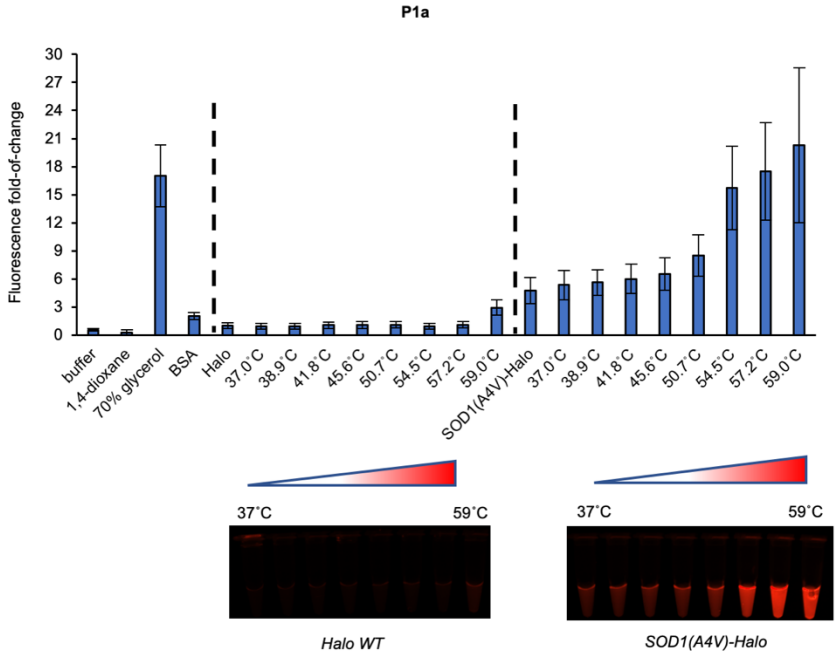

Figure S11. Fluorescence intensities for **P1a** (5 μM) measured in the thermodynamically stable HaloTag protein (42 μM) and aggregation-prone SOD1(A4V)-Halo protein (42 μM) at different temperature. For the HaloTag protein, fluorescence signal of **P1a** did not significantly turn on even at 59˚C. For SOD1(A4V), however, an increase of fluorescence intensity was observed at 54.5˚C. Samples were loaded into PCR tubes to enable a 20-minture incubation at different temperatures using C1000 Thermal Cycler (Bio-Rad), followed by imaging with Gel Doc™ EZ system (Bio-Rad). Fluorescence was recorded using the Tecan infinite M1000Pro fluorescence microplate reader.

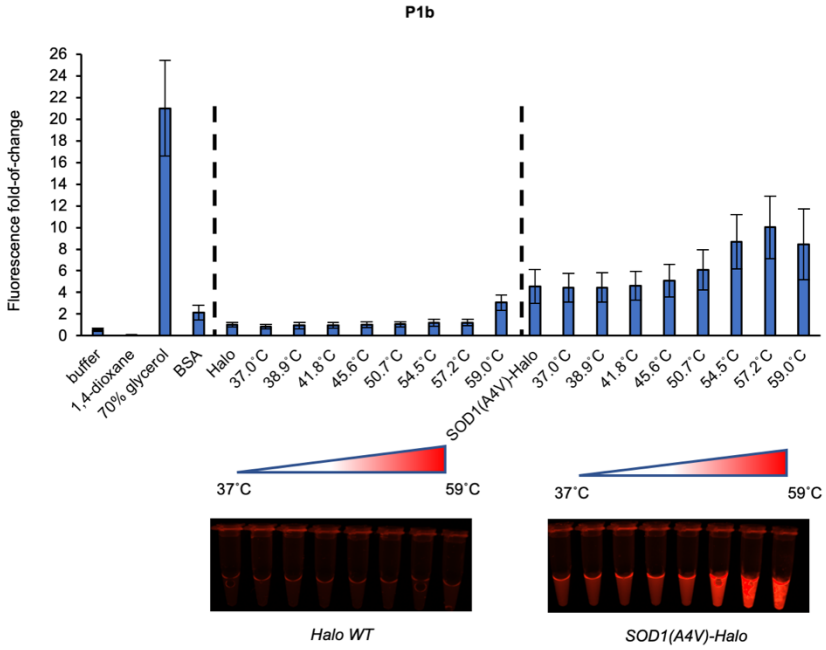

Figure S12. Fluorescence intensities for **P1b** (5 μM) measured in HaloTag protein (42 μM) and aggregation-prone SOD1(A4V)-Halo protein (42 μM) at different temperature. The fluorescence turn-on of **P1b** in aggregation prone SOD1(A4V) protein peaked at 57.2˚C and stopped increasing at 59 ºC, indicating that the fluorescence signal of **P1b** is predominantly coming from low viscosity misfolded protein oligomers. Samples were loaded into PCR tubes to enable a 20-minture incubation using C1000 Thermal Cycler (Bio-Rad) at different temperatures, followed by imaging with Gel DocTM EZ system (Bio-Rad). Fluorescence was recorded using the Tecan infinite M1000Pro fluorescence microplate reader.

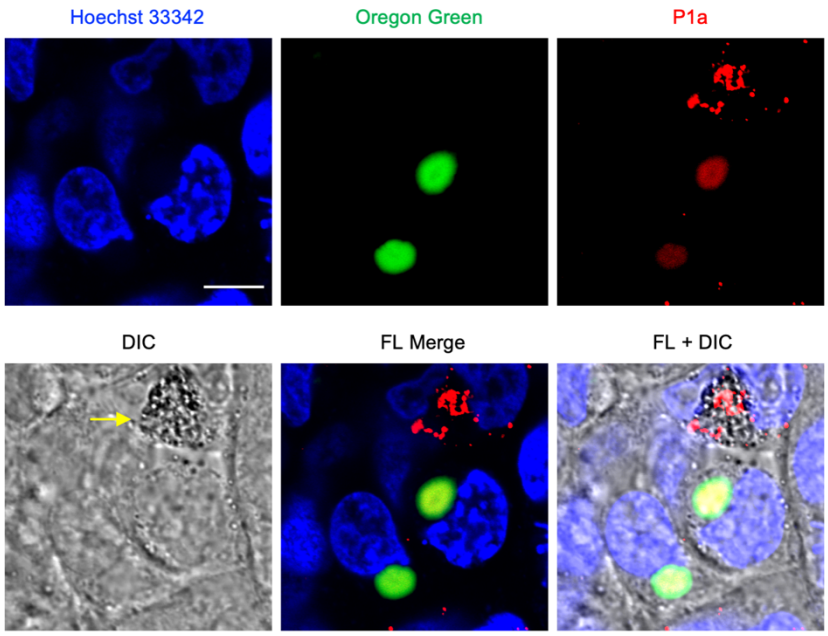

Figure S13. Dual-probe labelling experiment suggested the low cell membrane permeability of the positively charged **P1a**. HEK293T cells were transiently transfected with Htt-110Q-Halo and labelled with the membrane permeable HaloTag® Oregon Green® Ligand (0.5 μM, Promega) and **P1a** (0.5 μM). Live cell imaging was carried out using the Olympus FV1000 confocal microscope. Hoechst 33342, Oregon Green and **P1a** were excited using 405 nm, 458 nm and 543 nm lasers respectively. **P1a** has 1 net positive charge, which reduces the cell permeability. Meanwhile, extracellular **P1a** exhibited high fluorescence when binds with cell debris (yellow arrow, DIC channel). Scale bar: 10 μm.

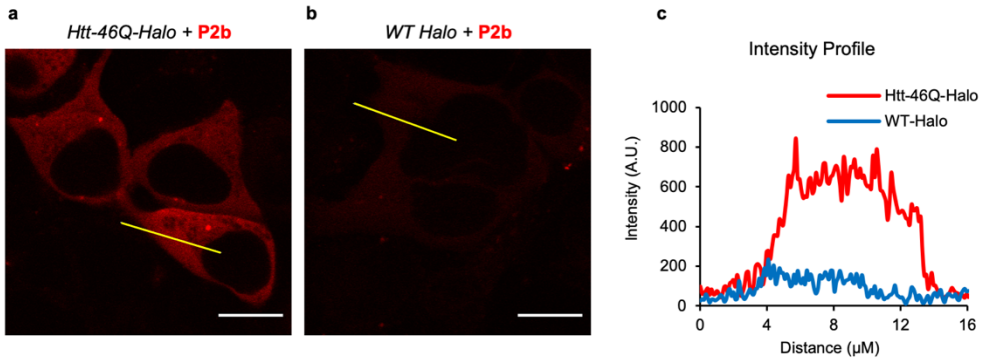

Figure S14. Quantification of fluorescence intensity profiles revealed low background fluorescence signal during live-cell imaging. (**a-b**) Images of Htt-46Q-Halo and WT Halo labelled with **P2b** (Figure 5c) were quantified along the yellow line. All pictures were taken with identical parameters using Olympus FV1000 confocal microscope. Scale bar: 10 μm. (**c**) Intensity profiles of Htt-46Q-Halo and WT Halo along the yellow lines in **a-b**. Despite its low *x* value (0.26), **P2b** exhibit a 4-fold fluorescence intensity increase upon the formation of Htt-46Q oligomers (red curve: ~600 A.U.) compared with the WT Halo control (blue curve ~150 A.U.).

SUPPORTING INFORMATION

Table S1. Solvent composition and viscosity of ethylene glycol and glycerol mixture.

Composition Glycerol *vol*%	30% Glycerol	50% Glycerol	60% Glycerol	70% Glycerol	80% Glycerol
Viscosity (mPa·s)	81	183	283	426	621

SUPPORTING INFORMATION

Table S2. Quantum yield of fluorophores in organic solvents.

	ThT	1a	1b	2a	2b	3a	3b
1.4-dioxane*	0.003	0.058	0.024	0.001	0.011	0.094	0.28
Ethyl Acetate	0.0006	0.008	0.003	N.D.	0.0006	0.006	0.26
Acetone	0.0003	0.014	0.006	0.0002	0.001	0.001	0.037
Methanol	0.0005	0.018	0.009	0.0003	0.003	0.001	0.023
DMSO	0.001	0.059	0.015	0.001	0.004	0.003	0.057
Ethylene Glycol	0.003	0.11	0.16	0.003	0.012	0.010	0.074
Glycerol	**0.16**	**0.75**	**0.51**	**0.03**	**0.08**	**0.19**	**0.65**

*90 *vol*% dioxane in water is used for benzothiazolium and HBI scaffolds to avoid aggregation caused quenching.

SUPPORTING INFORMATION

Table S3. Fluorescence lifetime of reported RBFs.

	Single exponential fitting			Double exponential fitting					
Probe	Solvent	t (ns)	Std (ps)	A_1 (%)	t_1 (ns)	Std (ps)	A_2 (%)	t_2 (ns)	Std (ps)
ThT	30 mPa.s	0.36	3	-	-	-	-	-	-
	1078 mPa.s	0.37	3	-	-	-	-	-	-
1a	30 mPa.s	0.36	1	-	-	-	-	-	-
	1078 mPa.s	1.16	2	18.45	0.31	18	81.55	1.26	3
1b	30 mPa.s	0.57	4	44.98	0.07	6	55.02	0.71	6
	1078 mPa.s	1.14	5	27.01	0.08	8	72.99	1.27	6
2a	30 mPa.s	0.17	3	-	-	-	-	-	-
	1078 mPa.s	0.38	2	-	-	-	-	-	-
2b	30 mPa.s	0.20	2	-	-	-	-	-	-
	1078 mPa.s	0.64	2	-	-	-	-	-	-
3a	30 mPa.s	0.22	1	98.71	0.21	4	1.29	0.70	90
	1078 mPa.s	1.00	2	28.54	0.52	20	71.46	1.14	4
3b	30 mPa.s	0.13	3	-	-	-	-	-	-
	1078 mPa.s	0.93	6	-	-	-	-	-	-

*Double fitting data showing negative amplitude were omitted.

SUPPORTING INFORMATION

Table S4. Calculated quantum yield (QY) of **ThT**, **1a** and **1b** at different viscosity and calculated percentage quantum yield (QY%) using QY at 1000 mPa·s as a reference.

Viscosity (mPa·s)	1	100	200	300	400	500	600	700	800	900	1000
ThT (QY)	0.00	0.03	0.04	0.06	0.08	0.09	0.11	0.12	0.13	0.15	0.16
QY% vs. in 1000 mPa·s	0.4%	16.2%	28.0%	38.5%	48.4%	57.8%	66.7%	75.4%	83.8%	92.0%	100.0%
1a (QY)	0.02	0.25	0.35	0.43	0.50	0.56	0.61	0.66	0.71	0.75	0.79
QY% vs. in 1000 mPa·s	3.0%	31.1%	44.2%	54.3%	62.8%	70.3%	77.2%	83.4%	89.3%	94.8%	100.0%
1b (QY)	0.06	0.25	0.31	0.35	0.38	0.41	0.43	0.46	0.48	0.49	0.51
QY% vs. in 1000 mPa·s	11.3%	48.3%	60.2%	68.4%	74.9%	80.3%	85.1%	89.4%	93.2%	96.7%	100.0%

*Quantum yield was calculated using Föster-Hoffmann equation, $log\emptyset = xlog\eta + C$, in which *x* and C are 0.79 and -3.17 for **ThT**, 0.51 and -1.62 for **1a**, 0.32 and -1.24 for **1b**.

*Data labelled in green indicate the largest fluorescence signal change in the corresponding viscosity region among this class of fluorophore.

4. Synthetic Methods

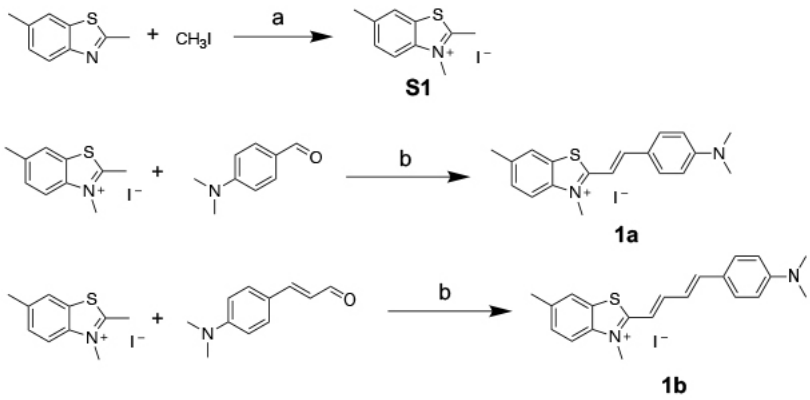

Scheme S1. Synthesis of benzothiazole fluorophores. (**a**) 1.0 eq. of 2,6-dimethylbenzothazole was dissolved in MeOH. Iodomethane (1.1 eq.) was added into the reaction and stirred overnight at 60˚C. Product was precipitated out from the reaction. Compounds **S1** were further purified by vacuum filtration and washed with cold MeOH. (**b**) 1 eq of **S1** was dissolved in MeOH, aldehyde (1.1 eq.) was added to the reaction. Catalytic amount of NaOH (0.05 eq.) was added to the reaction and stirred overnight at room temperature. Compound **1a** and **1b** were precipitated out from the reaction and further purified by vacuum filtration and washed with cold MeOH and ethyl acetate.

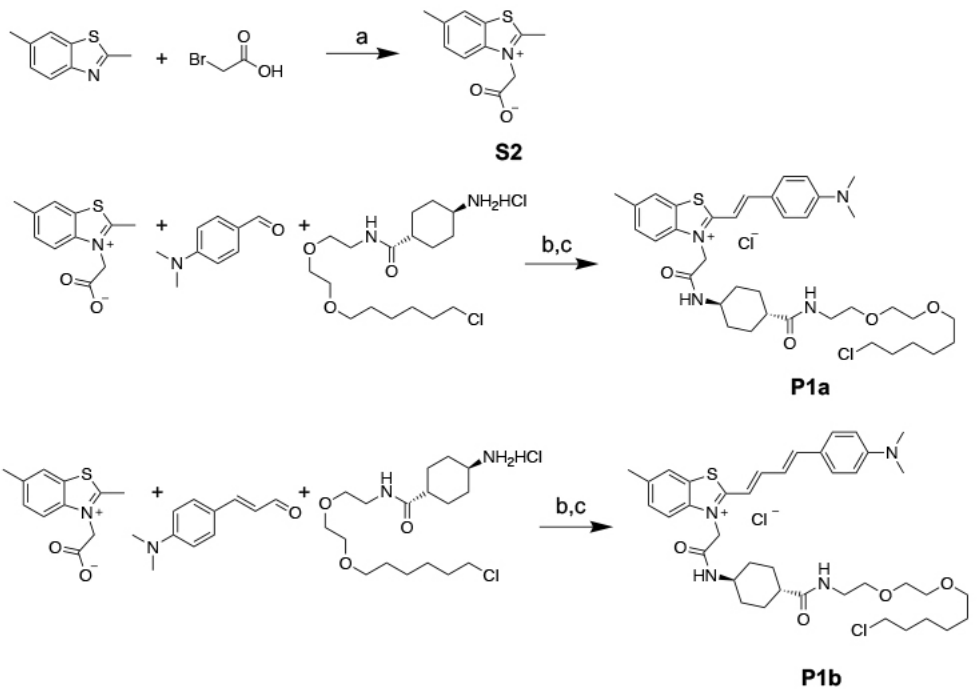

Scheme S2. Synthesis of benzothiazole Halo-Tag substrate. (a) 1.0 eq. of 2,6-dimethylbenzothazole was dissolved in toluene. Bromoacetic acid (1.5 eq.) was added into the reaction. The reaction was heated to reflux overnight. Product was precipitated out from the reaction. Compounds **S2** were further purified by vacuum filtration and washed with toluene. (b) 1.0 eq. of **S2** was dissolved in MeOH, aldehyde (1.1 eq.) was added to the reaction. Catalytic amount of NaOH (0.05 eq.) was added to the reaction and stirred overnight at room temperature. Products were precipitated out from the reaction, filtered and carried out with step (c) without purification. (c) In a round bottom flask, products from (b) were dissolved in dry DMF and mixed with 1.5 eq. N-(3-Dimethylaminopropyl)-N'-ethylcarbodiimide hydrochloride, 1.5 eq. 1-Hydroxybenzotriazole hydrate and 5.0 eq triethylamine. The reaction was stirred at room temperature for 30 min. 2.0 eq. of cyclohexane linker[4] was added the reaction and stirred at room temperature for overnight. Compound **P1a** and **P1b** were further purified by Agilent 1260 Infinity High Performance Liquid Chromatography.

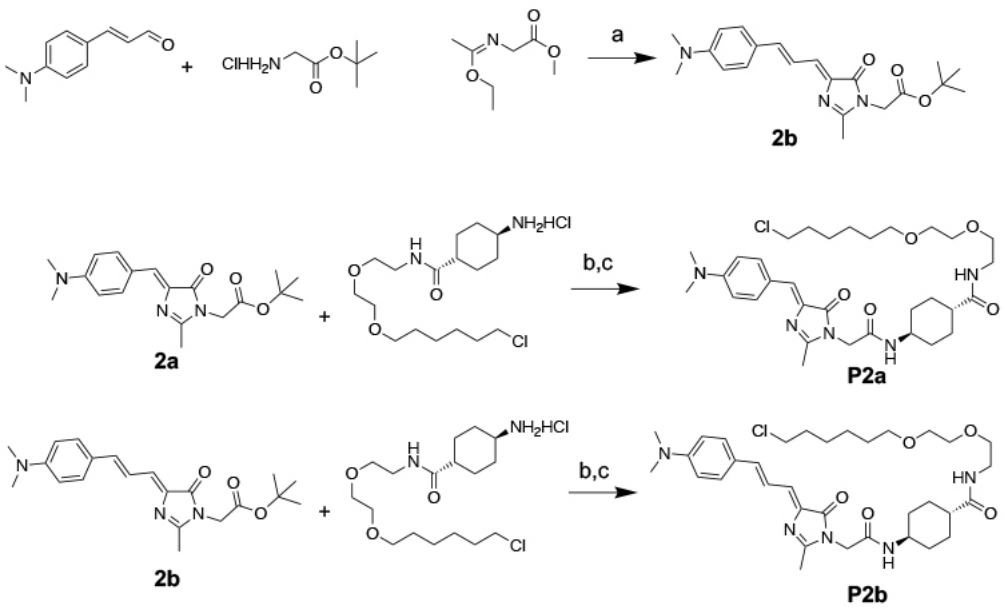

Scheme S3. Synthesis of HBI fluorophores. (a) 4-Dimethylaminocinnamaldehyde (1.0 eq.) was dissolved in EtOH. Glycine tert-butyl ester hydrochloride (1.1 eq.) and NaOH (1.1 eq.) was added to the reaction and stirred at room temperature for 2 hours. imidate[4] (1.0 eq.) was freshly prepared and added to the reaction. The reaction was stirred at room temperature overnight. The reaction was dried in vacuo to remove EtOH and extracted with ethyl acetate against water. The organic layer was collected, dried and further purified by column chromatography. (Ethyl acetate : Hexane = 2 : 1, rf = 0.3). **2a** was synthesized according to a published procedure[6]. (b) **2a** (or **2b**) and trifluoroacetic acid (6.0 eq.) was combined in DCM and stirred for 3 hours. The reaction was dried *in vacuo* proceed to the next step without purification. (c) products from (b) were dissolved in dry DMF and mixed with 1.5 eq. N-(3-Dimethylaminopropyl)-N'-ethylcarbodiimide hydrochloride, 1.5 eq. 1-Hydroxy-benzotriazole hydrate and 5.0 eq triethylamine. The reaction was stirred at room temperature for 30 min. 2.0 eq. of cyclohexane linker was added the reaction and stirred at room temperature for overnight. Compound **P2a** and **P2b** were further purified by Agilent 1260 Infinity High Performance Liquid Chromatography.

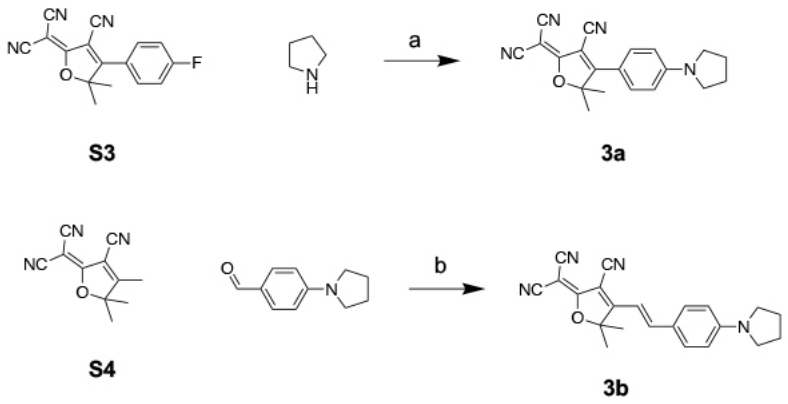

Scheme S4. Synthesis of DCDHF fluorophores. (a) **S3** was synthesized according to a published protocol[7]. 2.0 eq. of pyrrolidine was dissolved in pyridine, followed by adding 1.0 eq. of **S3.** The solution turned orange immediately, and **3a** was precipitated out from the solution. This reaction was stirred for another 2 hours at room temperature. Product **3a** was purified by vacuum filtration and washed with diluted HCl to remove excess pyridine. (b) **S4** was synthesized according to a published protocol[8]. 1.0 eq. of **S4** and 1.0 eq. of 4-(1-Pyrrolidino)benzaldehyde was dissolved in THF : EtOH = 4 : 1 solvent. 1.0 eq. of ammonium acetate was then added into the reaction in one portion. The reaction was kept under dark and stirred at room temperature overnight. 3b was precipitate out from the solution and further separated by vacuum filtration and washed with cold EtOH.

5. Characterization

S1 2,3,6-trimethylbenzo[d]thiazol-3-ium iodide
1H NMR (400 MHz, DMSO-d6) δ 8.23 (s, 1H), 8.18 (d, J = 8.7 Hz, 1H), 7.72 (dd, J = 8.7, 1.2 Hz, 1H), 4.19 (s, 3H), 3.16 (s, 3H), 2.53 (s, 3H). ^{13}C NMR (101 MHz, DMSO-d6) δ 175.98, 139.77, 138.33, 130.54, 128.74, 123.73, 116.35, 36.23, 20.98, 17.07. Calcd, 178.0685, Obsd, 178.0684.

S2 2-(2,6-dimethylbenzo[*d*]thiazol-3-ium-3-yl)acetate
^{1}H NMR (500 MHz, DMSO-d6) δ 8.32 (s, 1H), 8.21 (d, J = 8.7 Hz, 1H), 7.72 (dd, J = 8.8, 1.3 Hz, 1H), 5.80 (s, 2H), 3.22 (s, 3H), 2.52 (s, 3H). ^{13}C NMR (126 MHz, DMSO-d6) δ 177.87, 166.60, 139.37, 138.59, 130.97, 128.69, 124.11, 116.20, 50.06, 21.02, 17.05. $[M+H]^+$ Calcd, 222.0583, Obsd, 222.0576.

S3 2-(3-cyano-4-(4-fluorophenyl)-5,5-dimethylfuran-2(5H)-ylidene)malononitrile
^{1}H NMR (500 MHz, DMSO-d6) δ 7.91 (dd, *J* = 7.4, 5.3 Hz, 2H), 7.53 (t, *J* = 8.3 Hz, 2H), 1.75 (s, 6H). ^{13}C NMR (126 MHz, DMSO-d6) δ 177.06, 176.95, 164.54 (d, J = 253.4 Hz), 131.37, 131.30, 123.93, 123.91, 116.96, 116.78, 112.19, 111.32, 110.99, 103.23, 100.60, 55.63, 24.51. $[M+H]^+$ Calcd, 280.0881, Obsd, 280.0875.

S4 2-(3-cyano-4,5,5-trimethylfuran-2(5H)-ylidene)malononitrile
^{1}H NMR (500 MHz, $CDCl_3$) δ 2.37 (s, 3H), 1.63 (s, 6H). ^{13}C NMR (126 MHz, $CDCl_3$) δ 182.72, 175.26, 111.06, 110.44, 108.99, 104.76, 99.83, 58.40, 24.36, 14.23. $[M-H]^-$ Calcd, 198.0673, Obsd, 198.0670.

1a 2-(4-(dimethylamino)styryl)-3,6-dimethylbenzo[*d*]thiazol-3-ium iodide
^{1}H NMR (500 MHz, DMSO-d6) δ 8.09 (s, 1H), 8.06 - 7.96 (m, 2H), 7.89 (d, J = 8.9 Hz, 2H), 7.64 - 7.56 (m, 2H), 6.84 (d, J = 9.0 Hz, 2H), 4.21 (s, 3H), 3.10 (s, 6H), 2.50 (s, 3H). ^{13}C NMR (126 MHz, DMSO-d6) δ 170.35, 153.25, 149.46, 139.96, 137.69, 132.53, 129.93, 126.77, 123.17, 121.36, 115.50, 111.82, 106.27, 35.45, 20.82. Calcd, 309.1420, Obsd, 309.1419.

1b 2-(4-(4-(dimethylamino)phenyl)buta-1,3-dien-1-yl)-3,6-dimethylbenzo[*d*]thiazol-3-ium iodide
^{1}H NMR (500 MHz, DMSO-d6) δ 8.11 (s, 1H), 8.02 (d, J = 8.6 Hz, 1H), 7.93 (dd, J = 14.5, 11.0 Hz, 1H), 7.66 - 7.59 (m, 1H), 7.52 (d, J = 8.9 Hz, 2H), 7.41 (d, J = 15.0 Hz, 1H), 7.29 (d, J = 14.6 Hz, 1H), 7.18 (dd, J = 15.0, 11.0 Hz, 1H), 6.78 (d, J = 8.9 Hz, 2H), 4.13 (s, 3H), 3.03 (s, 6H), 2.50 (s, 3H). ^{13}C NMR (126 MHz, DMSO-d6) δ 169.48, 151.96, 150.47, 147.61, 139.92, 137.96, 130.27, 130.17, 127.13, 123.28, 122.77, 122.04, 115.68, 112.10, 112.02, 35.40, 20.86. Calcd, 335.1576, Obsd, 335.1576.

P1a 3-(2-((4-((2-(2-((6-chlorohexyl)oxy)ethoxy)ethyl)carbamoyl)cyclohexyl)amino)-2-oxoethyl)-2-(4-(dimethylamino)styryl)-6-methylbenzo[*d*]thiazol-3-ium chloride
^{1}H NMR (500 MHz, DMSO-d6) δ 8.66 (d, J = 7.8 Hz, 1H), 8.09 (d, J = 15.8 Hz, 2H), 7.86 (d, J = 8.9 Hz, 2H), 7.80 - 7.71 (m, 2H), 7.60 (d, J = 8.6 Hz, 1H), 7.54 (d, J = 15.2 Hz, 1H), 6.85 (d, J = 9.0 Hz, 2H), 5.48 (s, 2H), 3.61 (t, J = 6.6 Hz, 2H), 3.50 - 3.45(m, 5H), 3.37 (dt, J = 9.2, 6.3 Hz, 4H), 3.16 (q, J = 5.7 Hz,2H), 3.12 (s, 6H), 2.49 (s, 3H), 2.10 (t, J = 11.7 Hz, 1H), 1.85 (d, J = 9.8 Hz, 2H), 1.76 - 1.65 (m, 4H), 1.48 (p, J = 6.7 Hz, 2H), 1.42 - 1.19 (m, 8H). ^{13}C NMR (126 MHz, DMSO-d6) δ 174.70, 171.74, 163.07, 153.62, 150.38, 139.59, 137.89, 132.86, 130.29, 126.54, 123.56, 121.46, 114.66, 112.02, 105.97, 70.18, 69.59, 69.45, 69.09, 50.21, 48.10, 45.38, 42.92, 38.40, 32.02, 31.49, 29.08, 28.00, 26.12, 24.94, 20.91. Calcd, 683.3392, Obsd, 683.3386.

P1b 3-(2-((4-((2-(2-((6-chlorohexyl)oxy)ethoxy)ethyl)carbamoyl)cyclohexyl)amino)-2-oxoethyl)-2-(4-(4-dimethylamino)phenyl)buta-1,3-dien-1-yl)-6-methylbenzo[*d*]thiazol-3-ium chloride
^{1}H NMR (400 MHz, DMSO-d6) δ 8.98 (d, J = 7.7 Hz, 1H), 8.11 (s, 1H), 7.96 (dd, J = 14.5, 10.9 Hz, 1H), 7.90 (d, J = 8.7 Hz, 1H), 7.80 (t, J = 5.7 Hz, 1H), 7.60 (d, J = 8.7 Hz, 1H), 7.52 (d, J = 8.6 Hz, 2H), 7.43 (d, J = 15.0 Hz, 1H), 7.27 (d, J = 14.5 Hz, 1H), 7.12 (dd, J = 15.0, 11.0 Hz, 1H), 6.77 (d, J = 8.6 Hz, 2H), 5.45 (s, 2H), 3.61 (t, J = 6.6 Hz, 2H), 3.47 (d, J = 4.8 Hz, 5H), 3.40 - 3.34 (m, 4H), 3.17 (q, J = 5.9 Hz, 2H), 3.04 (s, 6H), 2.49 (s, 3H), 2.11 (s, 1H), 1.86 (d, J = 9.1 Hz, 2H), 1.76 - 1.66 (m, 4H), 1.47 (q, J = 6.9 Hz, 2H), 1.40 - 1.24 (m, 8H). ^{13}C NMR (101 MHz, DMSO-d6) δ 174.72, 170.87, 162.74, 152.19, 151.29, 148.39, 139.59, 138.11, 130.60, 130.46, 126.89, 123.57, 122.85, 122.08, 115.10, 112.11, 111.96, 70.16, 69.57, 69.42, 69.07, 50.16, 48.18, 45.35, 42.88, 38.37, 32.00, 31.40, 29.06, 27.99, 26.10, 24.91, 20.93. Calcd, 709.3549, Obsd, 709.3545.

2a tert-butyl 2-(4-(4-(dimethylamino)benzylidene)-2-methyl-5-oxo-4,5-dihydro-1*H*-imidazol-1-yl)acetate
^{1}H NMR (500 MHz, $CDCl_3$) δ 8.06 (d, J = 9.1 Hz, 2H), 7.09 (d, J = 8.5 Hz, 1H), 6.69 (d, J = 9.4 Hz, 2H), 4.27 (s, 2H), 3.04 (s, 6H), 2.30 (s, 3H), 1.47 (s, 9H). ^{13}C NMR (126 MHz, $CDCl_3$) δ 170.11, 166.90, 158.03, 151.56, 134.26, 129.41, 122.19, 111.72, 82.83, 42.14, 40.03, 27.98, 15.41. $[M+H]^+$ Calcd, 344.1896, Obsd, 344.1983

2b tert-butyl 2-(4-(3-(4-(dimethylamino)phenyl)allylidene)-5-oxo-4,5-dihydro-1*H*-imidazol-1-yl)acetate
^{1}H NMR (500 MHz, $CDCl_3$) δ 7.45 (d, J = 8.9 Hz, 2H), 7.39 (dd, J = 15.4, 11.8 Hz, 1H), 7.03 (d, J = 11.8 Hz, 1H), 6.96 (d, J = 15.4 Hz, 1H), 6.63 (d, J = 8.9 Hz, 2H), 4.25 (s, 2H), 2.99 (s, 6H), 2.28 (s, 3H), 1.46 (s, 9H). ^{13}C NMR (126 MHz, $CDCl_3$) δ 168.81, 166.76, 157.92, 151.18, 143.89, 136.12, 131.06, 129.47, 124.31, 118.51, 111.86, 82.87, 42.03, 40.09, 27.92, 15.24. $[M+H]^+$ Calcd, 370.2125,Obsd, 370.2124.

P2a *N*-(2-(2-((6-chlorohexyl)oxy)ethoxy)ethyl)-4-(2-(4-(4-(dimethylamino)benzylidene)-2-methyl-5-oxo-4,5-dihydro-1*H*-imidazol-1-yl)acetamido)cyclohexane-1-carboxamide

^{1}H NMR (500 MHz, $CDCl_3$) δ 8.07 (d, J = 8.5 Hz, 2H), 7.12 (s, 1H), 6.71 (d, J = 8.5 Hz, 2H), 6.07 - 5.88 (m, 2H), 4.21 (s, 2H), 3.72 (tdt, J = 12.0, 8.0, 4.1 Hz, 1H), 3.62 - 3.38 (m, 12H), 3.07 (s, 6H), 2.39 (s, 3H), 2.04 - 1.85 (m, 4H), 1.80 - 1.65 (m, 4H), 1.63 - 1.50 (m, 4H), 1.47 - 1.31 (m, 4H), 1.14 (m, 1H). ^{13}C NMR (126 MHz, $CDCl_3$) δ 175.00, 170.58, 166.30, 157.56, 151.89, 134.59, 133.56, 130.57, 121.84, 111.77, 71.27, 70.24, 70.00, 69.81, 48.21, 45.08, 44.76, 44.37, 40.05, 39.02, 32.51, 32.03, 29.46, 28.26, 26.69, 25.41, 15.59. $[M+H]^+$ Calcd, 618.3417, Obsd, 618.3415.

P2b *N*-(2-(2-((6-chlorohexyl)oxy)ethoxy)ethyl)-4-(2-(4-(3-(4-(dimethylamino)phenyl)allylidene)-2-methyl-5-oxo-4,5-dihydro-1*H*-imidazol-1-yl)acetamido)cyclohexane-1-carboxamide

^{1}H NMR (500 MHz, DMSO-d6) δ 8.20 (d, J = 7.7 Hz, 1H), 7.76 (t, J = 5.7 Hz, 1H), 7.48 (d, J = 8.9 Hz, 2H), 7.35 - 7.22 (m, 2H), 7.05 (d, J = 10.3 Hz, 1H), 6.76 (d, J = 8.9 Hz, 2H), 4.28 (s, 2H), 3.62 (t, J = 6.6 Hz, 2H), 3.51 - 3.44 (m, 5H), 3.37 (dt, J = 9.2, 6.3 Hz, 4H), 3.17 (q, J = 5.9 Hz, 2H), 3.01 (s, 6H), 2.35 (s, 3H), 2.07 (ddt, J = 15.4, 12.1, 3.3 Hz, 1H), 1.83 (dd, J = 13.1, 3.4 Hz, 2H), 1.77 - 1.66 (m, 4H), 1.48 (dt, J = 14.2, 6.7 Hz, 2H), 1.39 (m, 4H), 1.31 (m, 2H), 1.18 (q, J = 12.7 Hz, 2H). ^{13}C NMR (126 MHz, DMSO) δ 174.77, 165.10, 160.51, 159.15, 158.42, 151.53, 145.51, 135.46, 129.70, 123.60, 117.42, 112.17, 70.19, 69.59, 69.45, 69.10, 47.77, 45.39, 43.00, 42.31, 38.39, 32.03, 31.55, 29.09, 28.11, 26.14, 24.95, 14.53. $[M+H]^+$ Calcd, 644.3573, Obsd, 644.3568.

3a 2-(3-cyano-5,5-dimethyl-4-(4-(pyrrolidin-1-yl)phenyl)furan-2(5*H*)-ylidene)malononitrile

^{1}H NMR (500 MHz, DMSO-d6) δ 8.06 (d, J = 8.6 Hz, 2H), 6.79 (d, J = 8.6 Hz, 2H), 3.48 (m, 4H), 2.00 (m, 4H), 1.81 (s, 6H). ^{13}C NMR (126 MHz, DMSO-d6) δ 177.80, 174.34, 151.72, 132.41, 113.71, 113.64, 112.77, 112.57, 98.14, 88.94, 50.39, 47.75, 26.60, 24.68. $[M+H]^+$ Calcd, 331.1553, Obsd, 331.1550.

3b 2-(3-cyano-5,5-dimethyl-4-(4-(pyrrolidin-1-yl)styryl) furan-2(5*H*)-ylidene)malononitrile

^{1}H NMR (500 MHz, DMSO-d6) δ 7.93 (d, J = 15.7 Hz, 1H), 7.78 (d, J = 8.4 Hz, 2H), 6.86 (d, J = 15.7 Hz, 1H), 6.70 (d, J = 8.5 Hz, 2H), 3.44 (m, 4H), 1.99 (m, 4H), 1.75 (s, 6H). ^{13}C NMR (126 MHz, DMSO-d6) δ 177.29, 175.22, 151.33, 149.57, 133.13, 121.73, 113.51, 112.73, 112.68, 112.06, 107.72, 97.95, 91.17, 50.40, 47.66, 25.59, 24.73. $[M+H]^+$ Calcd, 357.1710, Obsd, 357.1706.

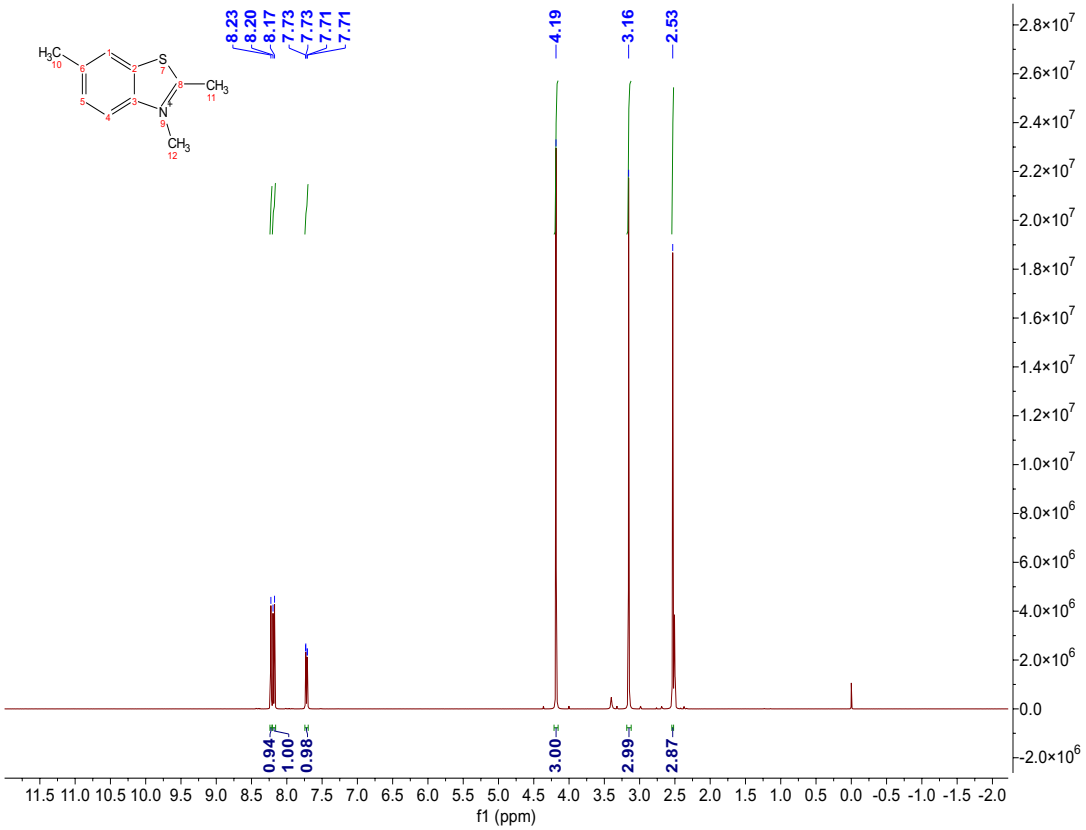
8.23
8.20
8.17
7.73
7.73
7.71
7.71
4.19
3.16
2.53
0.94
1.00
0.98
3.00
2.99
2.87
f1 (ppm)

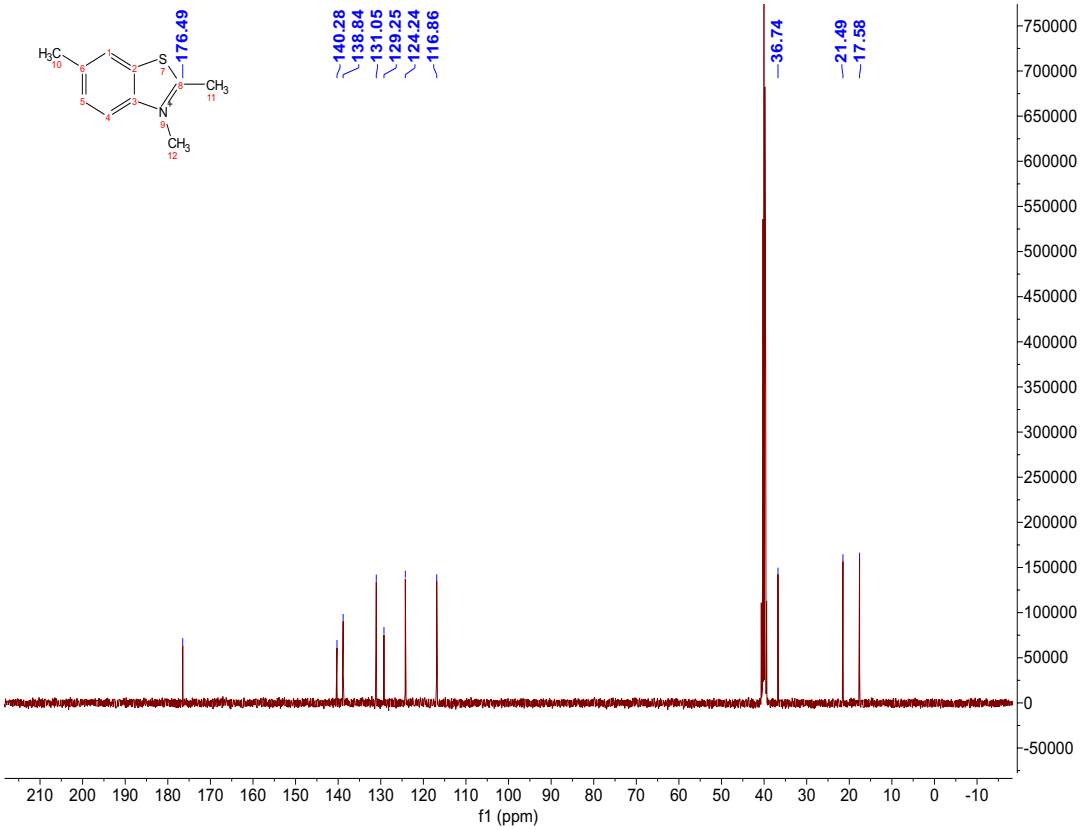
176.49
140.28
138.84
131.05
129.25
124.24
116.86
36.74
21.49
17.58
f1 (ppm)

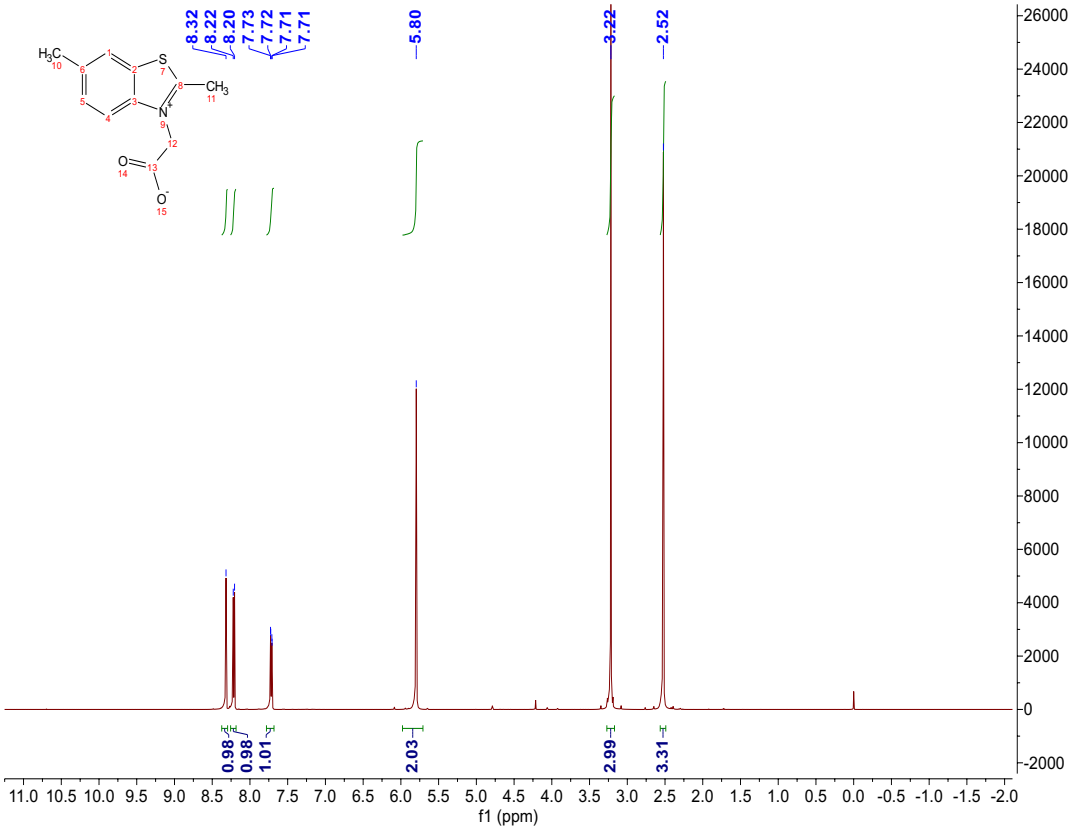
8.32
8.22
8.20
7.73
7.72
7.71
7.71
5.80
3.22
2.52
0.98
0.98
1.01
2.03
2.99
3.31
f1 (ppm)

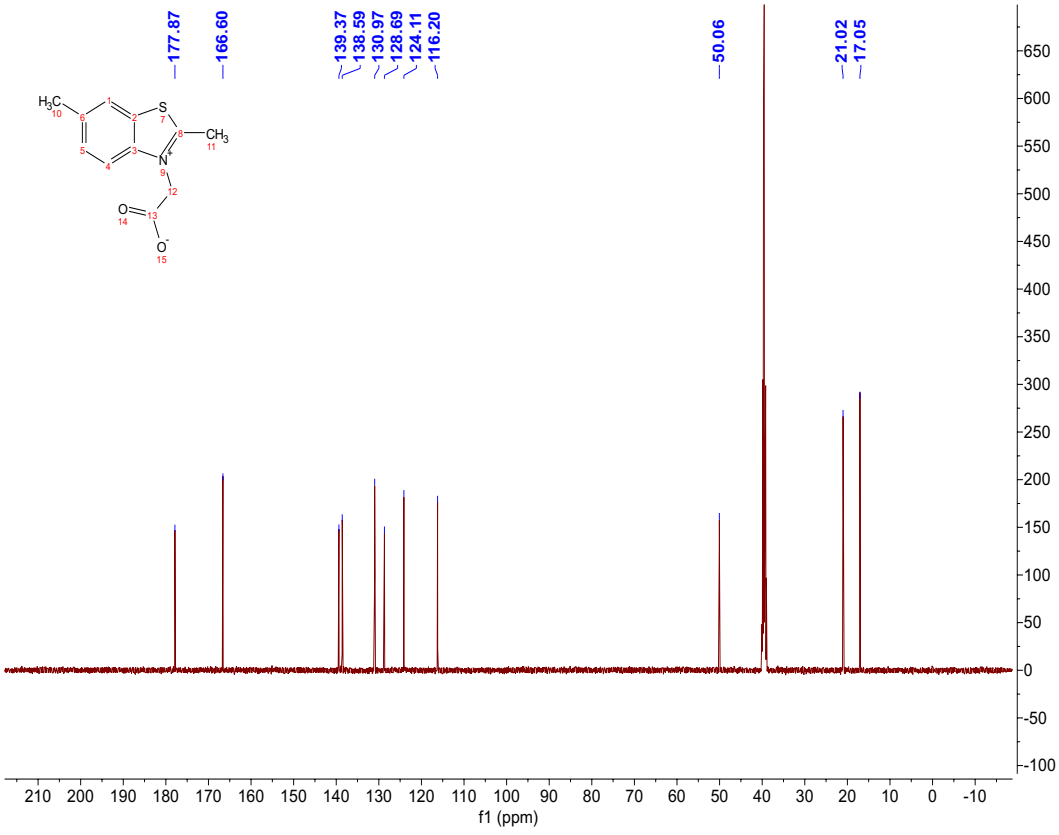
177.87
166.60
139.37
138.59
130.97
128.69
124.11
116.20
50.06
21.02
17.05
f1 (ppm)

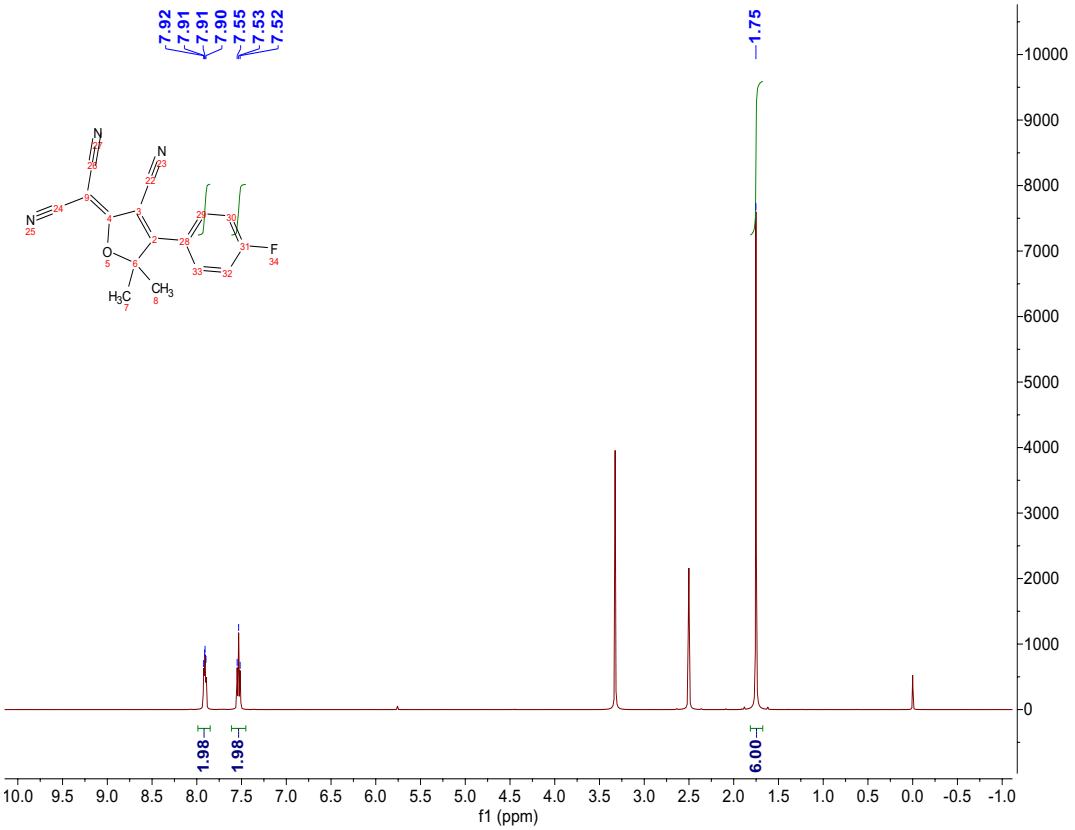
7.92
7.91
7.91
7.90
7.55
7.53
7.52
1.75
1.98
1.98
6.00
f1 (ppm)

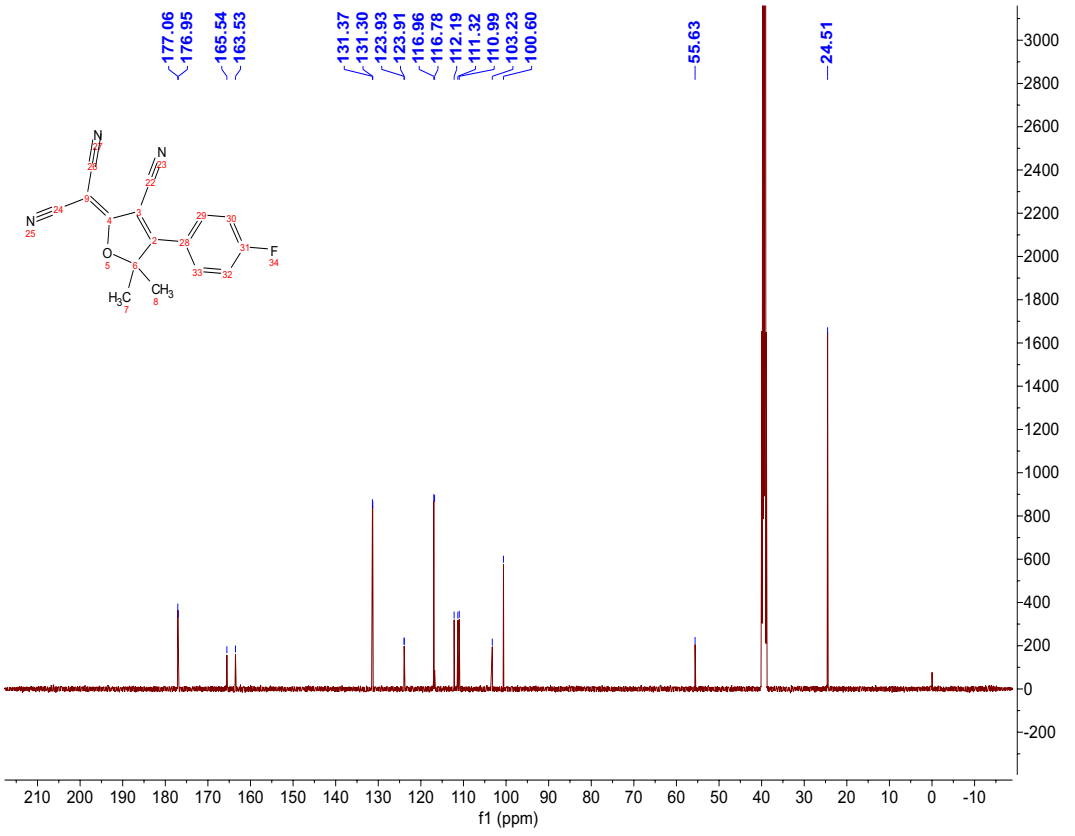
177.06
176.95
165.54
163.53
131.37
131.30
123.93
123.91
116.96
116.78
112.19
111.32
110.99
103.23
100.60
55.63
24.51
f1 (ppm)

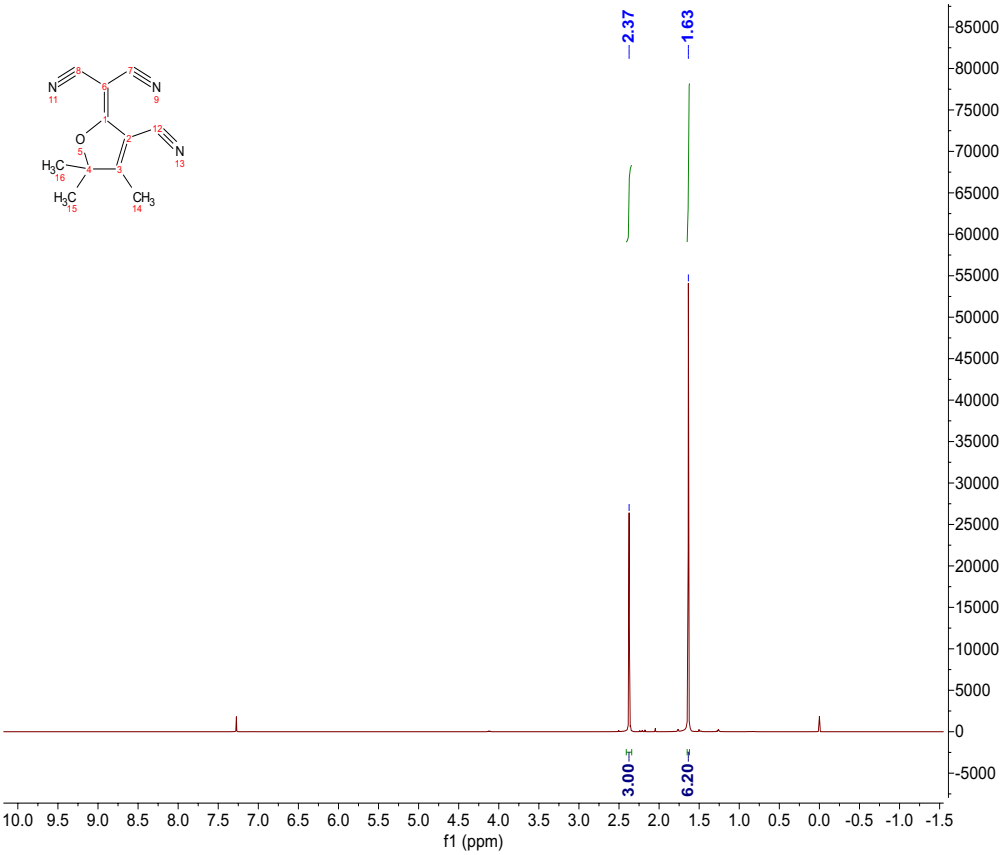
2.37
1.63
3.00
6.20
f1 (ppm)

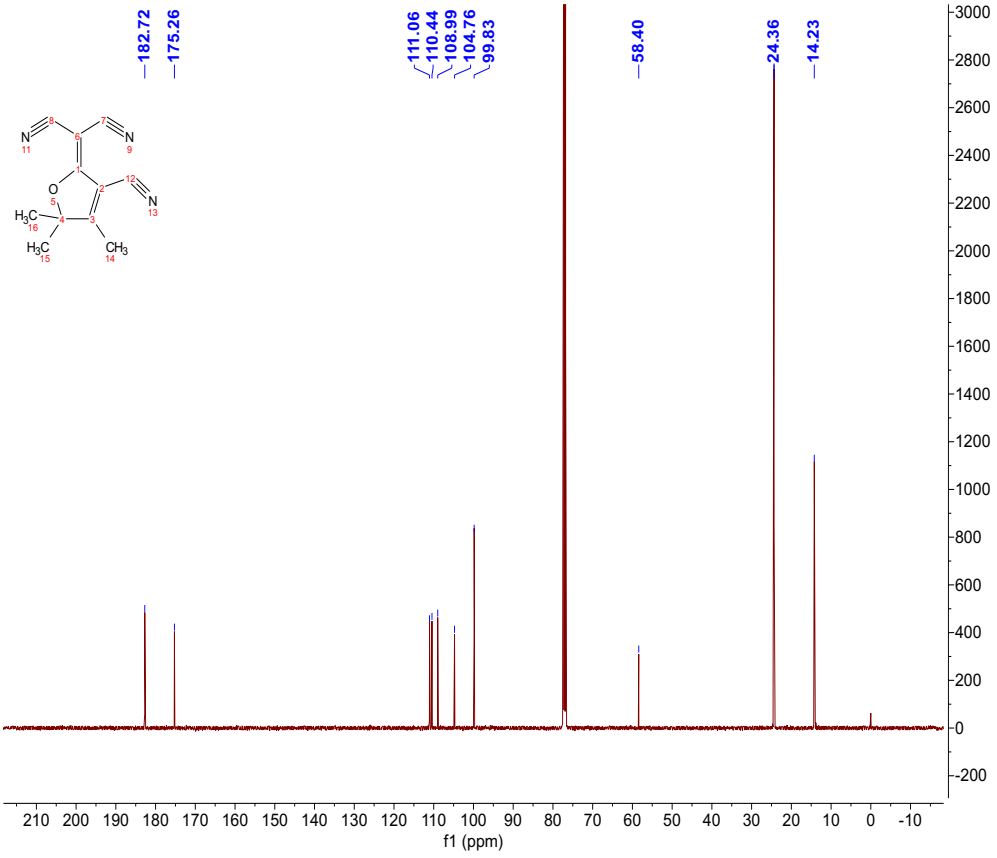
182.72
175.26
111.06
110.44
108.99
104.76
99.83
58.40
24.36
14.23
f1 (ppm)

SUPPORTING INFORMATION

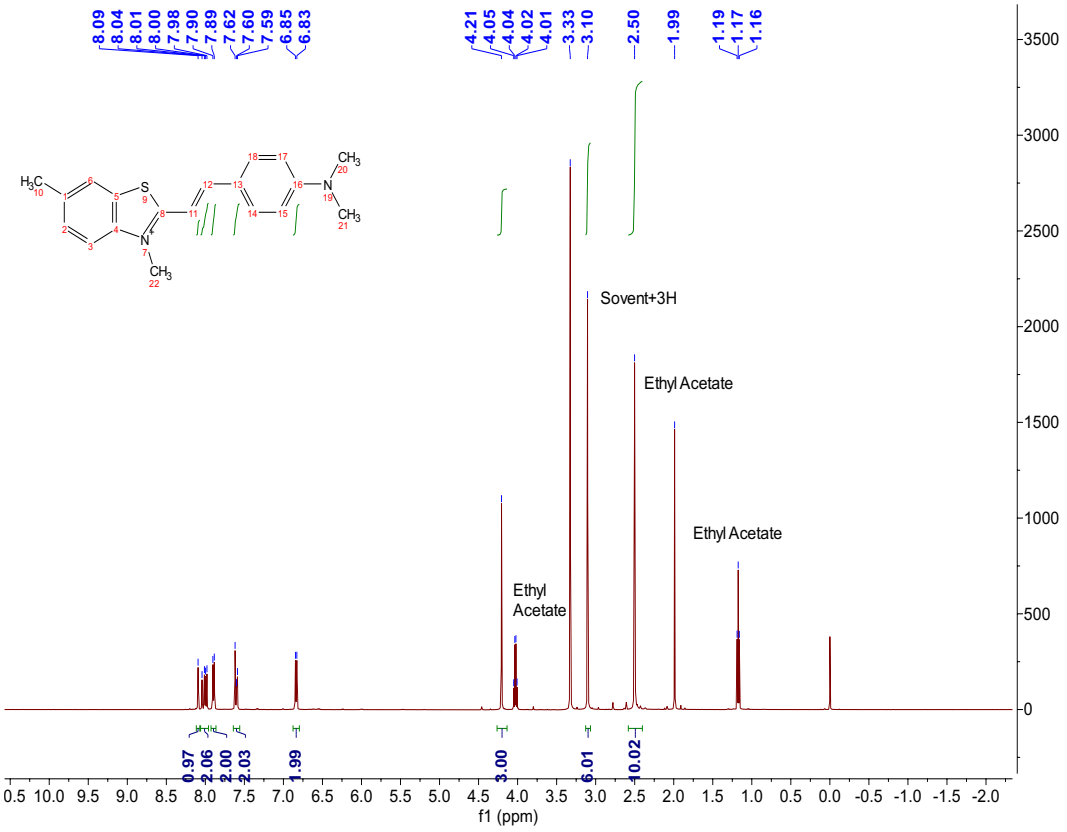

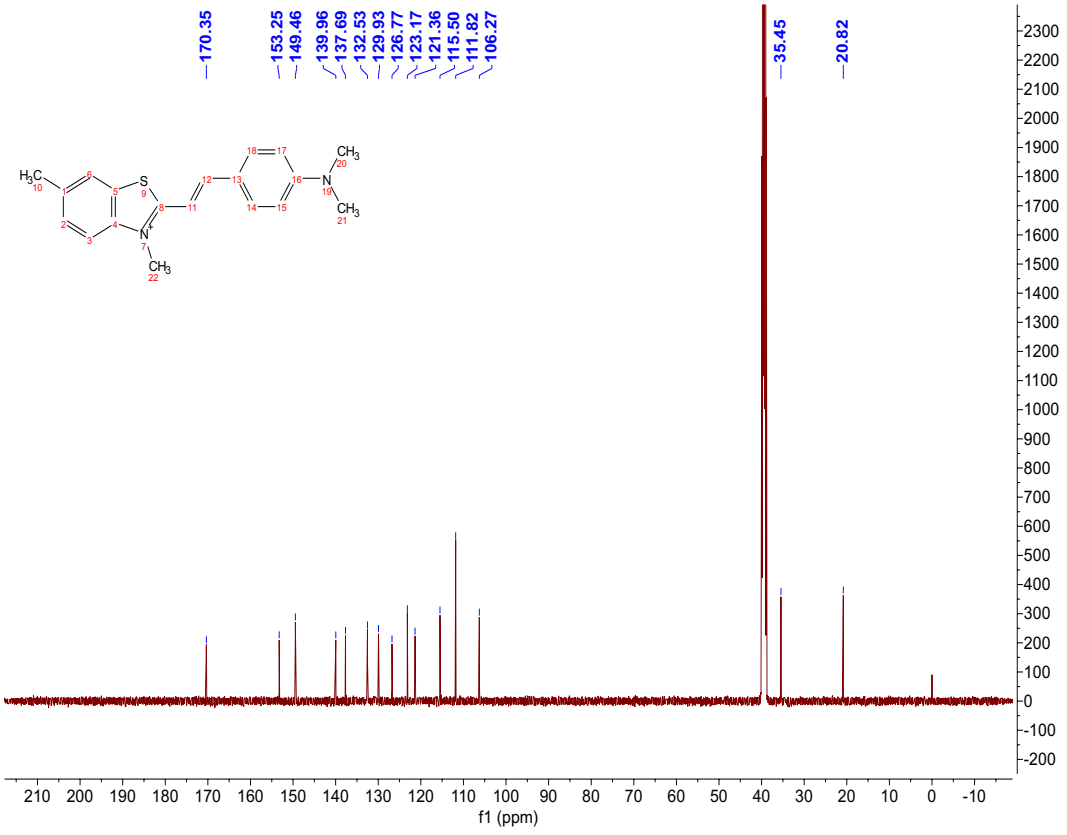

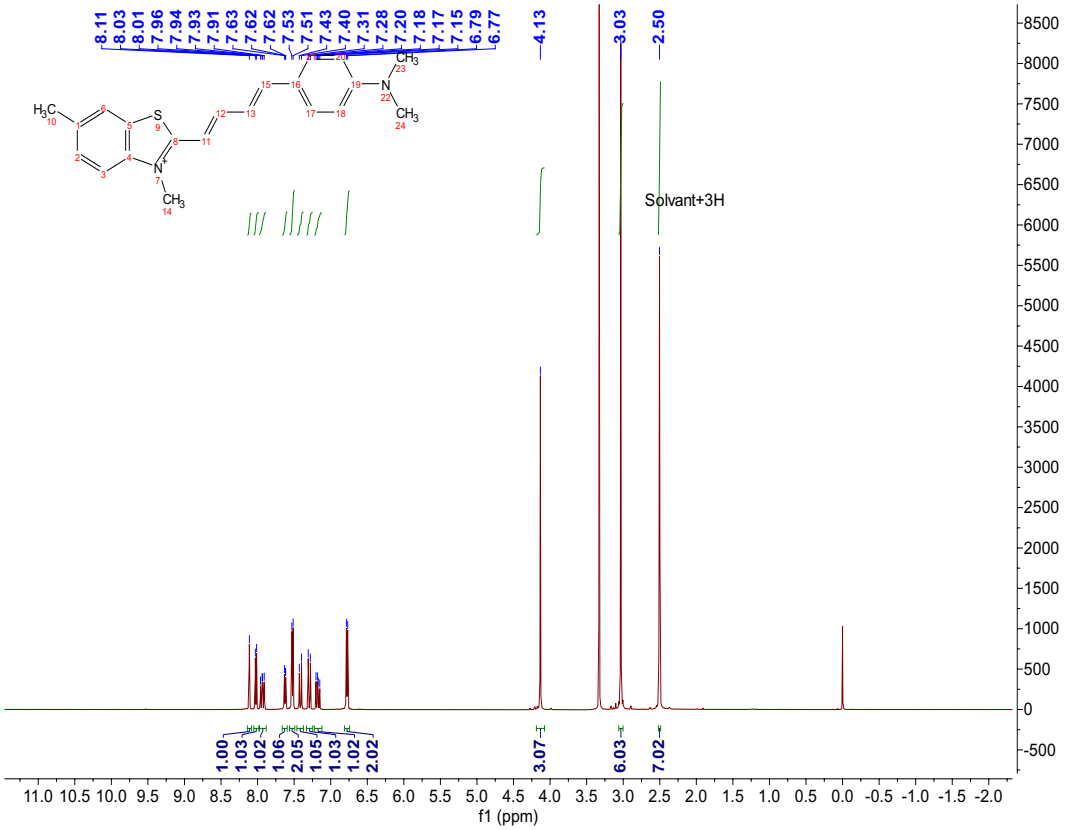
8.11
8.03
8.01
7.96
7.94
7.93
7.91
7.63
7.62
7.62
7.53
7.51
7.43
7.40
7.31
7.28
7.20
7.18
7.17
7.15
6.79
6.77
4.13
3.03
2.50
Solvant+3H
1.00
1.03
1.02
1.06
2.05
1.05
1.03
1.02
2.02
3.07
6.03
7.02
f1 (ppm)

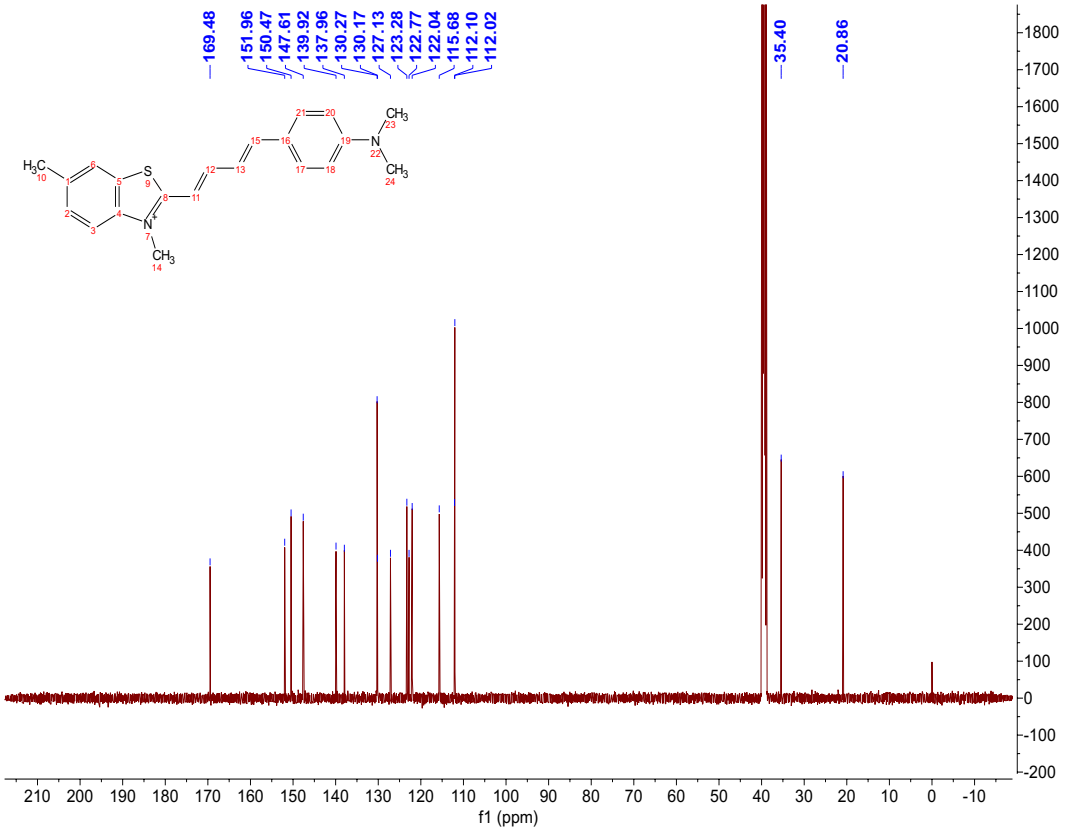
169.48
151.96
150.47
147.61
139.92
137.96
130.27
130.17
127.13
123.28
122.77
122.04
115.68
112.10
112.02
35.40
20.86
f1 (ppm)

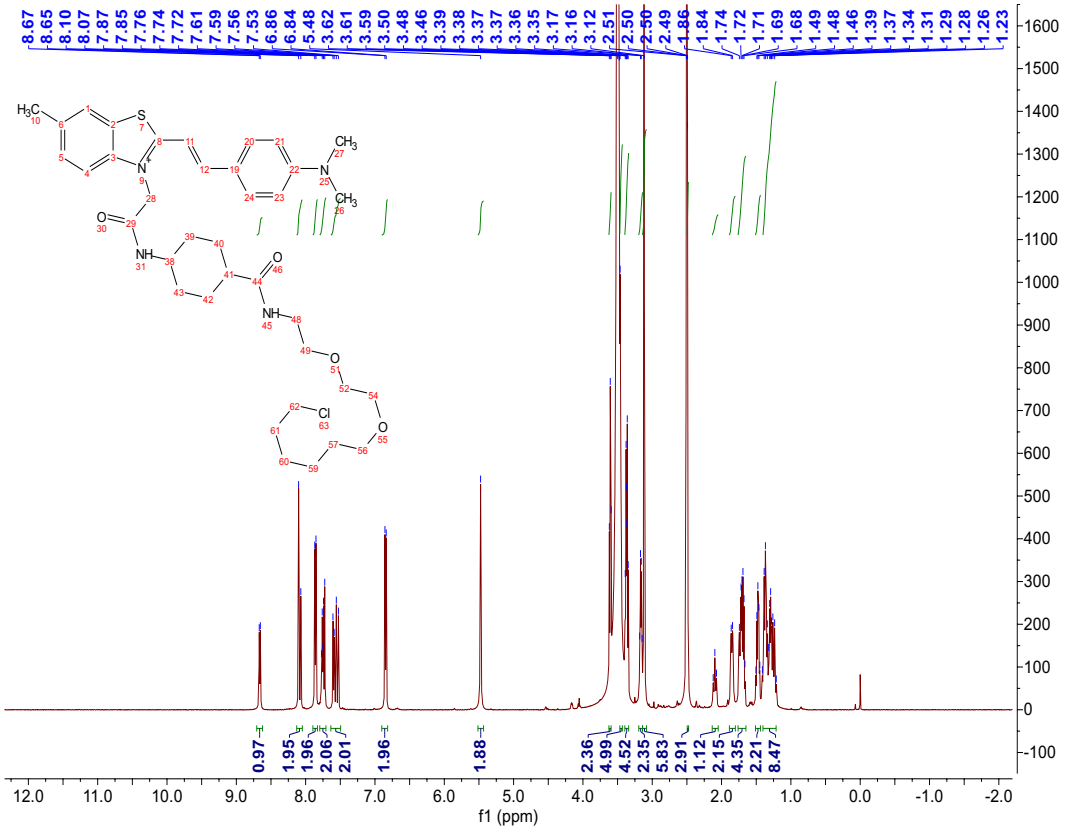
8.67 8.65 8.10 8.07 7.87 7.85 7.76 7.74 7.72 7.61 7.59 7.56 7.53 6.86 6.84 5.48 3.62 3.61 3.59 3.50 3.48 3.46 3.39 3.38 3.37 3.37 3.36 3.35 3.17 3.16 3.12 2.51 2.50 2.50 2.49 1.86 1.84 1.74 1.72 1.71 1.69 1.68 1.49 1.48 1.46 1.39 1.37 1.34 1.31 1.29 1.28 1.26 1.23
0.97 1.95 1.96 2.06 2.01 1.96 1.88 2.36 4.99 4.52 2.35 5.83 2.91 1.12 2.15 4.35 2.21 8.47
f1 (ppm)

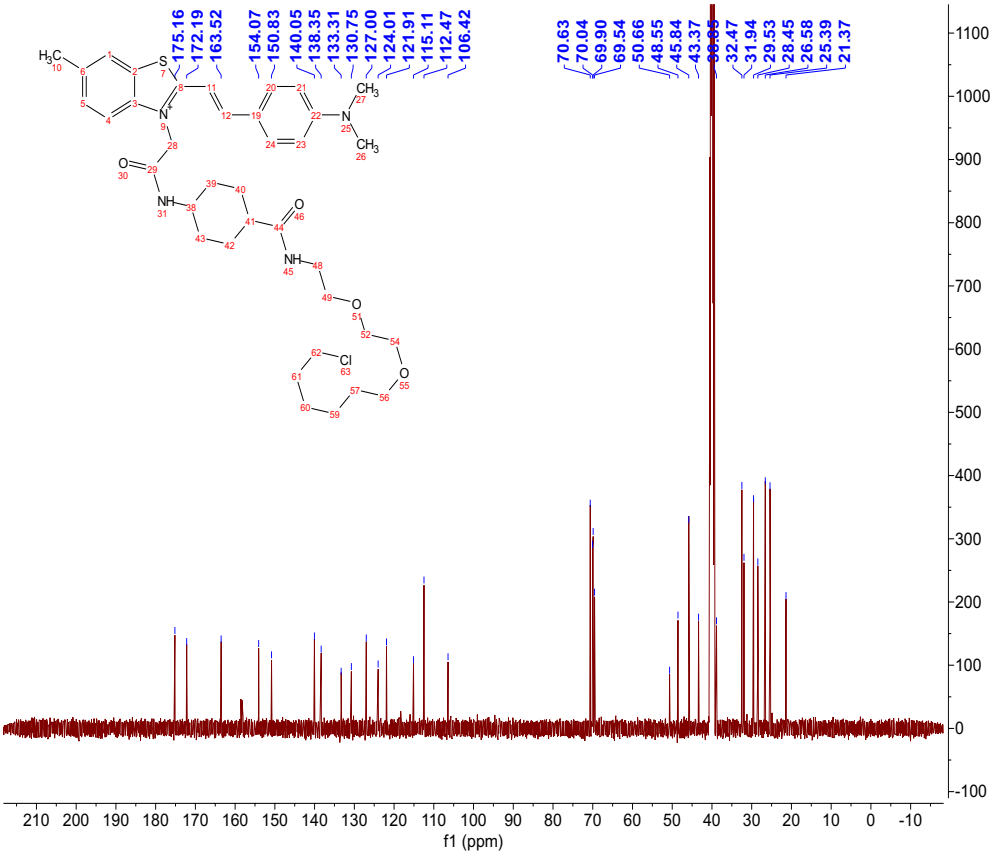
175.16 172.19 163.52 154.07 150.83 140.05 138.35 133.31 130.75 127.00 124.01 121.91 115.11 112.47 106.42
70.63 70.04 69.90 69.54 50.66 48.55 45.84 43.37 32.47 31.94 29.53 28.45 26.58 25.39 21.37
f1 (ppm)

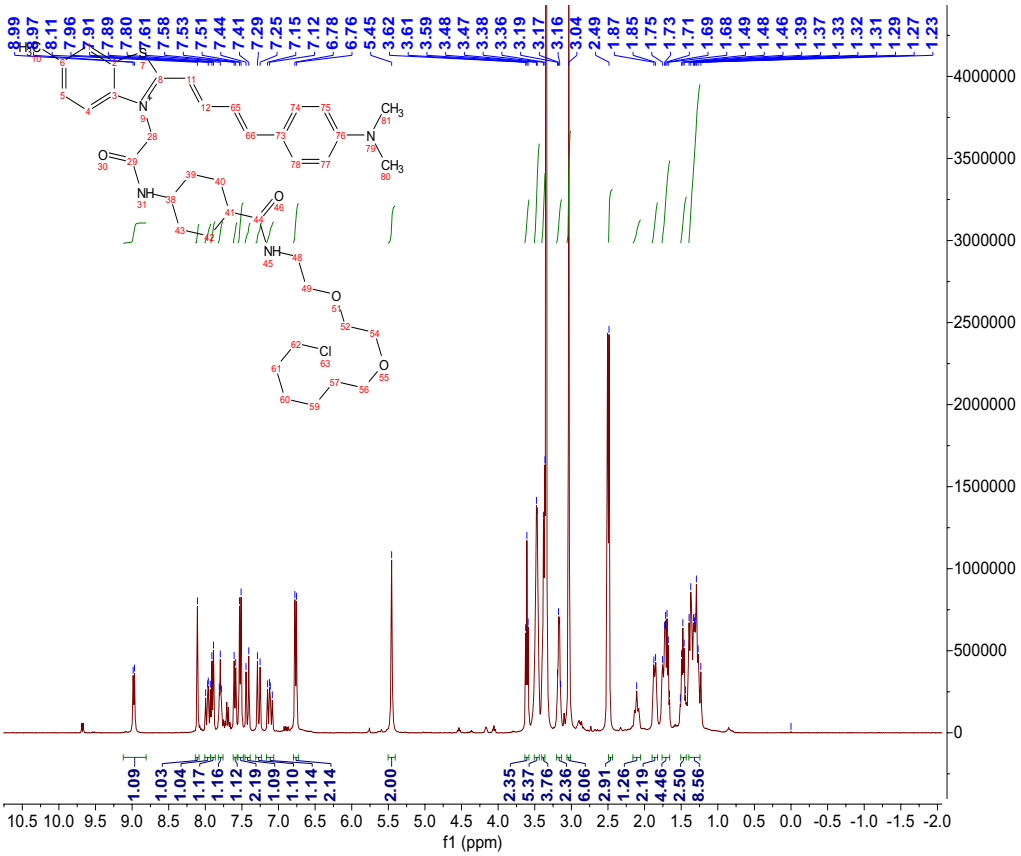
f1 (ppm)

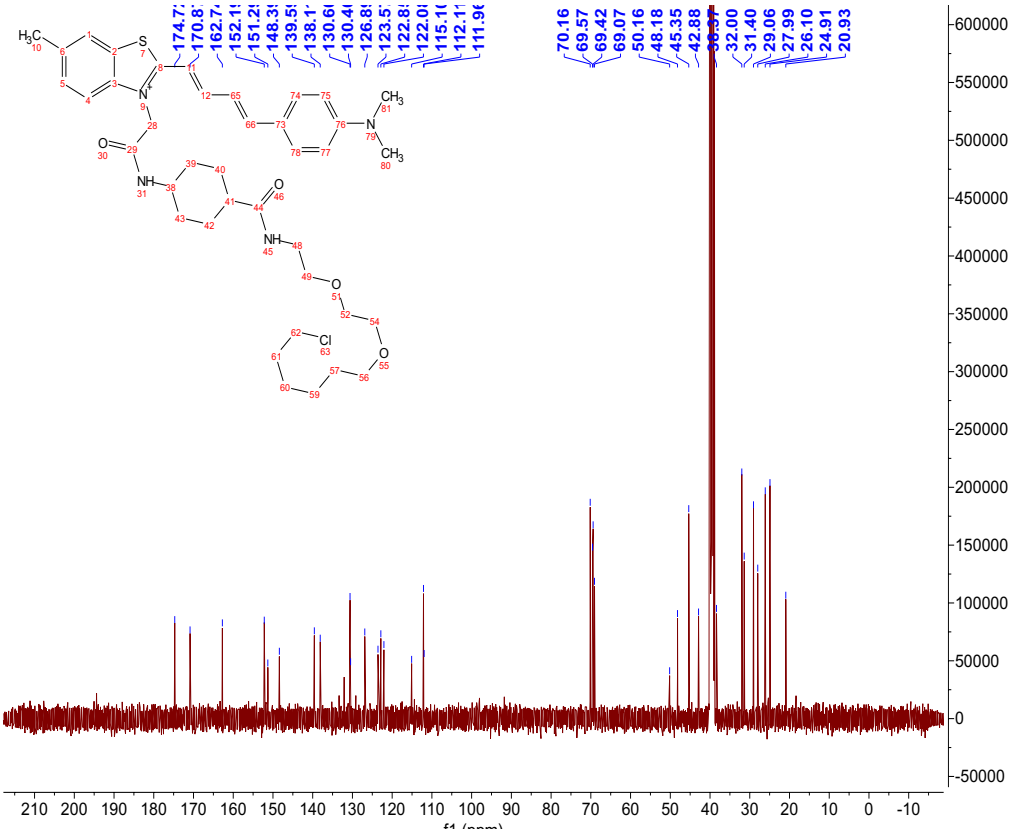

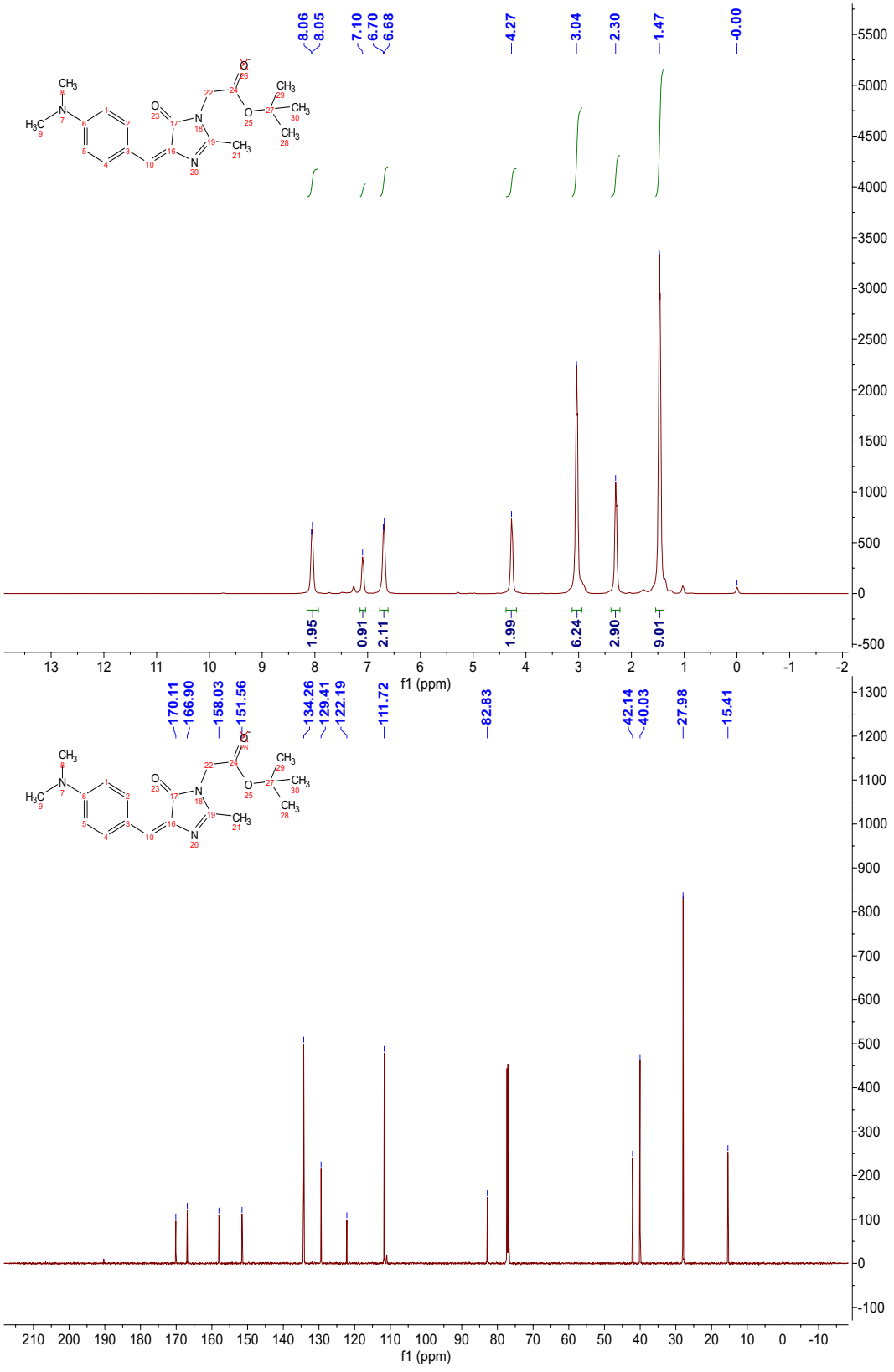
8.06
8.05
7.10
6.70
6.68
4.27
3.04
2.30
1.47
0.00
1.95
0.91
2.11
1.99
6.24
2.90
9.01
f1 (ppm)
170.11
166.90
158.03
151.56
134.26
129.41
122.19
111.72
82.83
42.14
40.03
27.98
15.41
f1 (ppm)

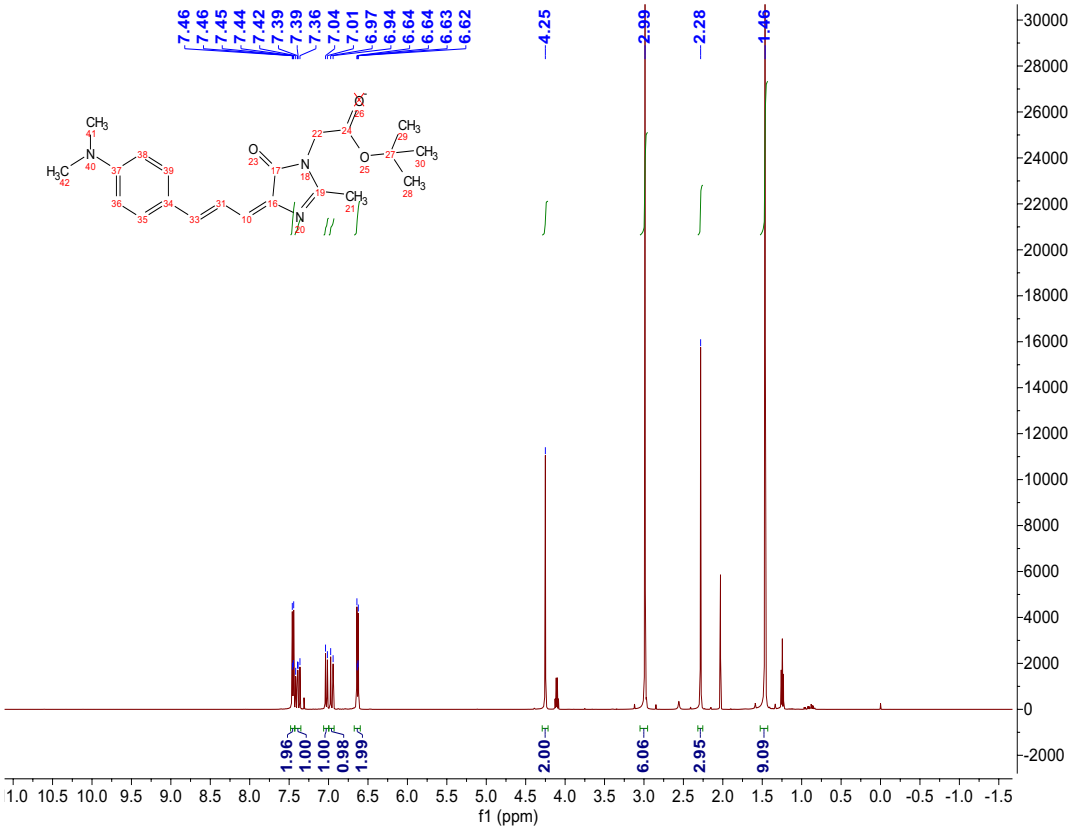
7.46
7.46
7.45
7.44
7.42
7.39
7.39
7.36
7.04
7.01
6.97
6.94
6.64
6.64
6.63
6.62
4.25
2.99
2.28
1.46
1.96
1.00
1.00
0.98
1.99
2.00
6.06
2.95
9.09
f1 (ppm)

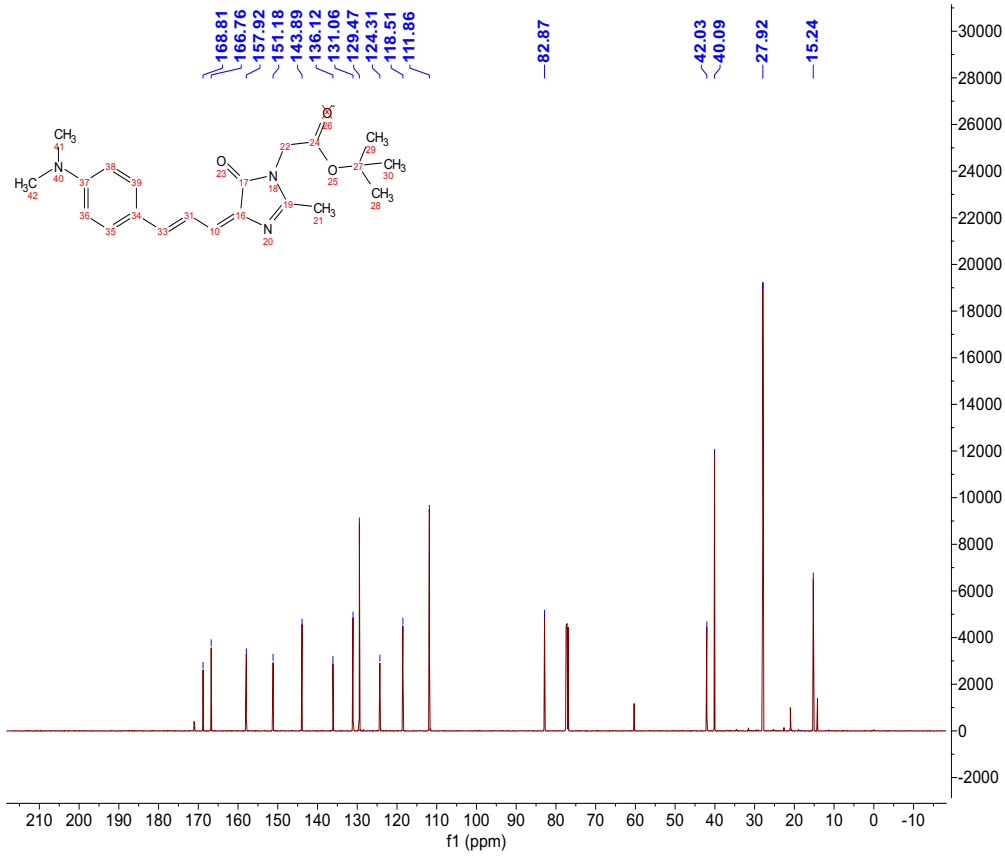
168.81
166.76
157.92
151.18
143.89
136.12
131.06
129.47
124.31
118.51
111.86
82.87
42.03
40.09
27.92
15.24
f1 (ppm)

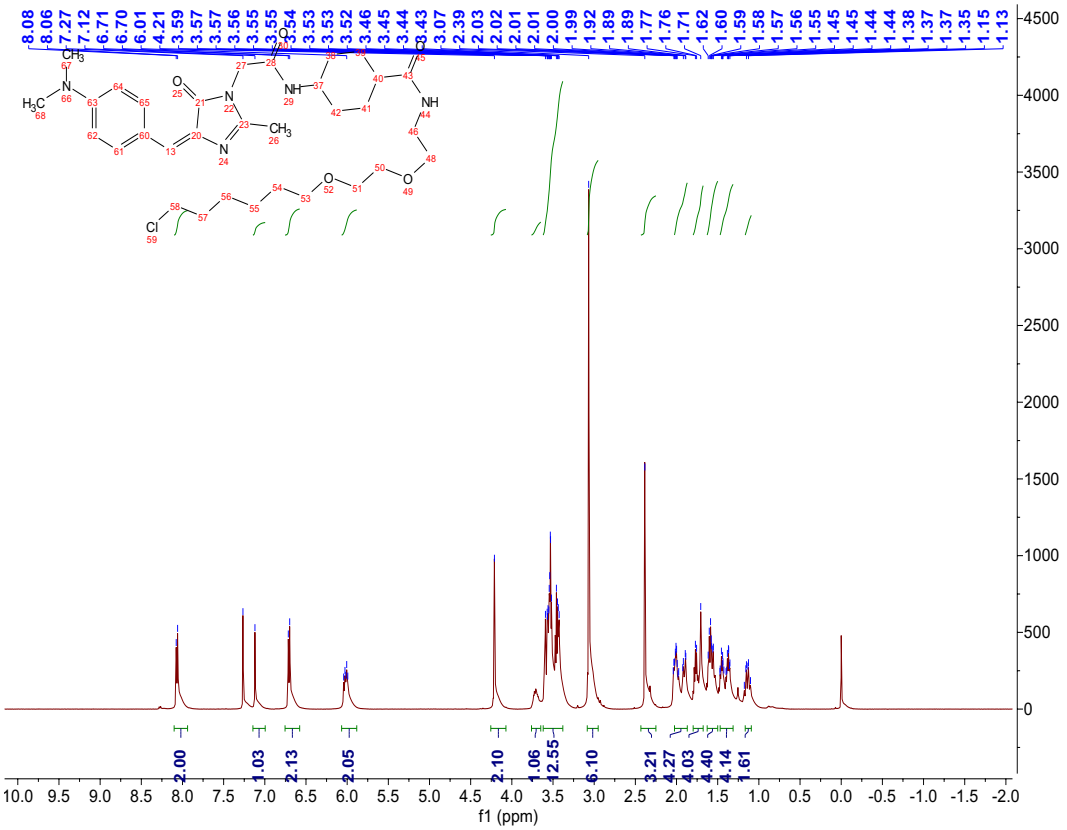
8.08 8.06 7.27 7.12 6.71 6.70 6.01 4.21 3.59 3.57 3.57 3.56 3.55 3.55 3.54 3.53 3.53 3.52 3.46 3.45 3.44 3.43 3.07 2.39 2.03 2.02 2.01 2.01 2.00 1.99 1.92 1.89 1.89 1.77 1.76 1.71 1.62 1.60 1.59 1.58 1.57 1.56 1.55 1.45 1.45 1.44 1.44 1.38 1.37 1.37 1.35 1.15 1.13
2.00 1.03 2.13 2.05 2.10 1.06 12.55 6.10 3.21 4.27 4.03 4.40 4.14 1.61
f1 (ppm)

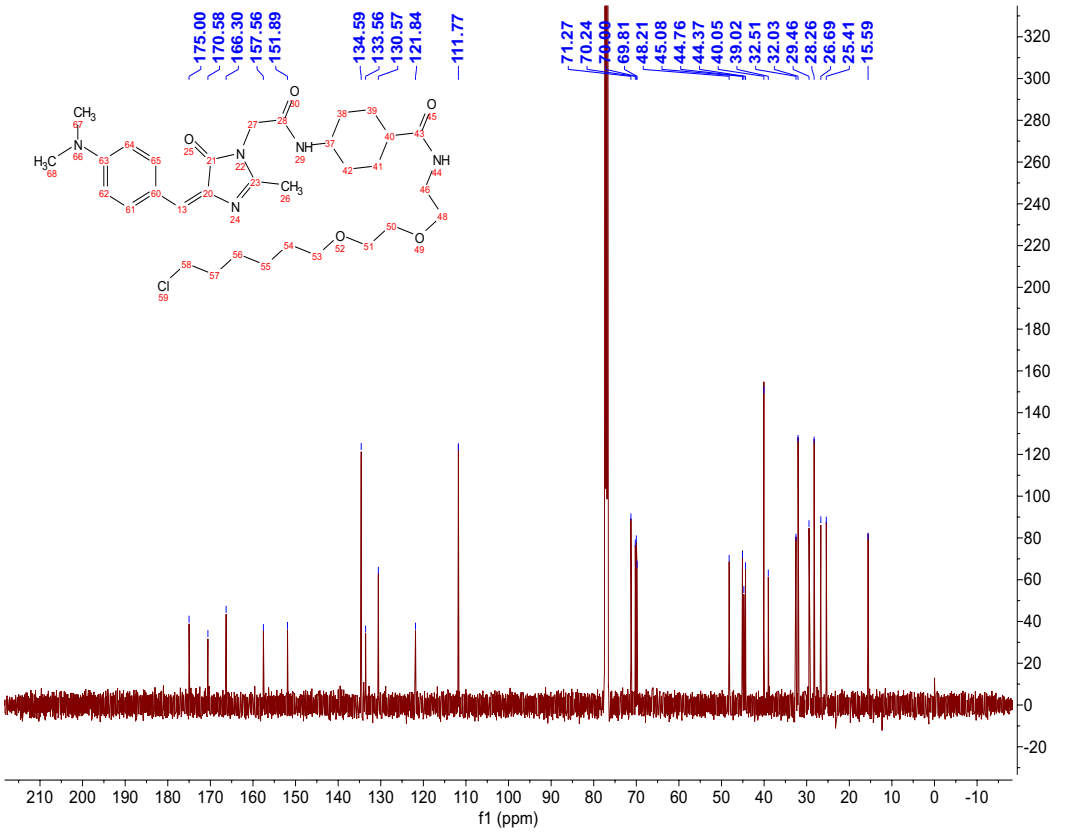
175.00 170.58 166.30 157.56 151.89 134.59 133.56 130.57 121.84 111.77 71.27 70.24 70.00 69.81 48.21 45.08 44.76 44.37 40.05 39.02 32.51 32.03 29.46 28.26 26.69 25.41 15.59
f1 (ppm)

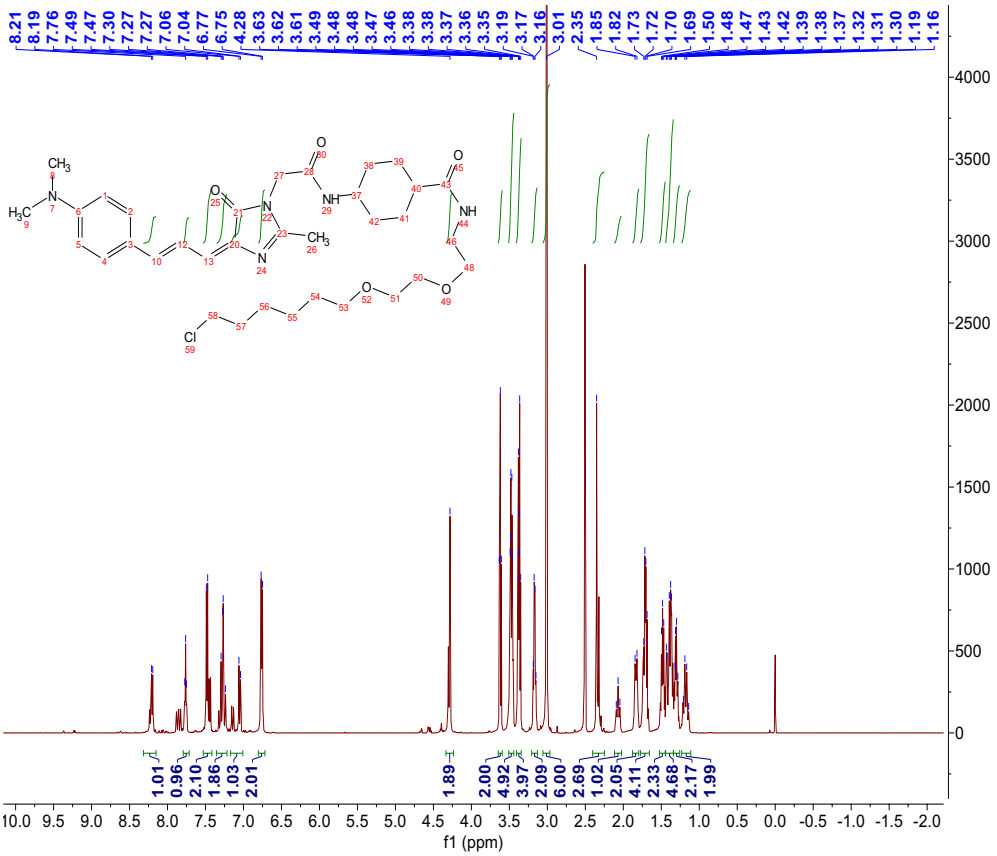
8.21 8.19 7.76 7.49 7.47 7.30 7.27 7.27 7.06 7.04 6.77 6.75 4.28 3.63 3.62 3.61 3.49 3.48 3.48 3.47 3.46 3.38 3.38 3.37 3.36 3.35 3.19 3.17 3.16 3.01 2.35 1.85 1.82 1.73 1.72 1.70 1.69 1.50 1.48 1.47 1.43 1.42 1.39 1.38 1.37 1.32 1.31 1.30 1.19 1.16
1.01 0.96 2.10 1.86 1.03 2.01 1.89 2.00 4.92 3.97 2.09 6.00 2.69 1.02 2.05 4.11 2.33 4.68 2.17 1.99
f1 (ppm)

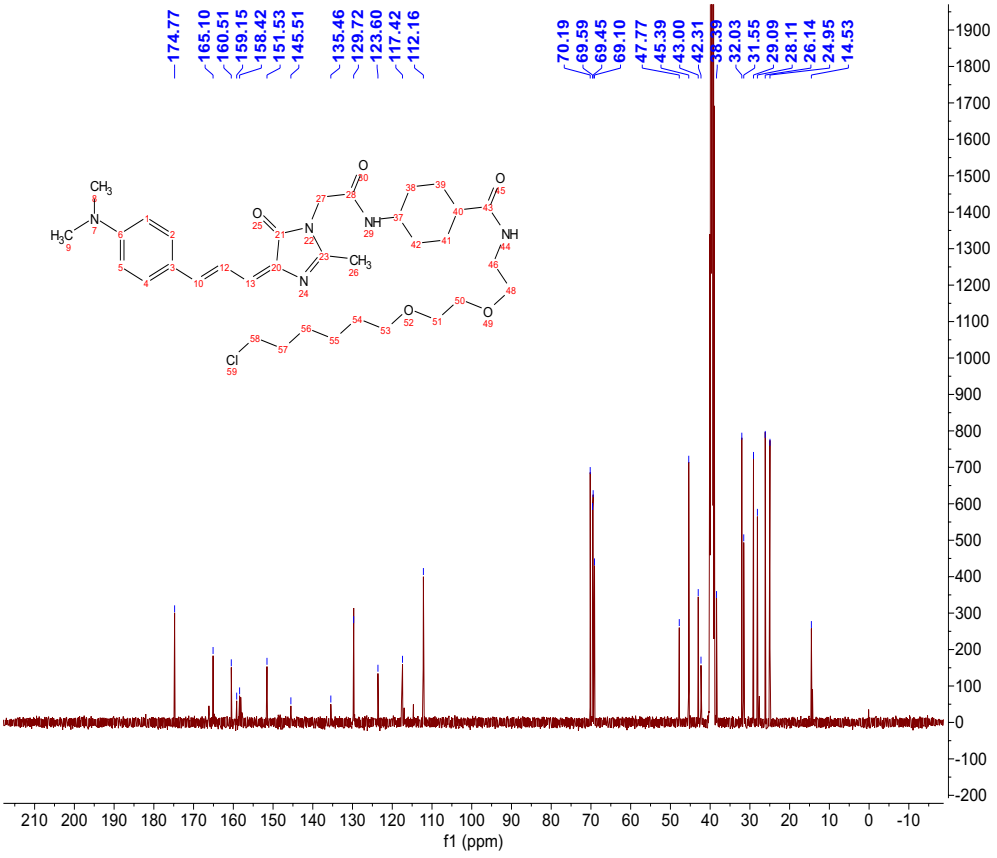
174.77 165.10 160.51 159.15 158.42 151.53 145.51 135.46 129.72 123.60 117.42 112.16 70.19 69.59 69.45 69.10 47.77 45.39 43.00 42.31 38.39 32.03 31.55 29.09 28.11 26.14 24.95 14.53
f1 (ppm)

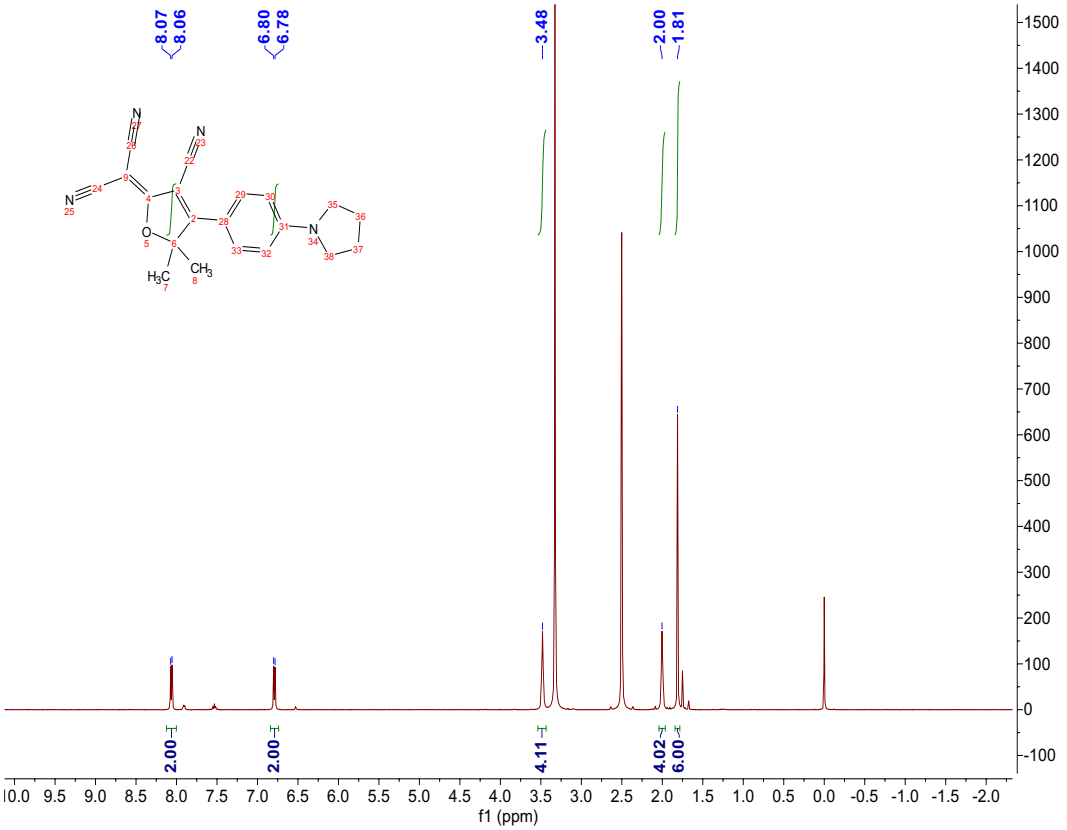
8.07
8.06
6.80
6.78
3.48
2.00
1.81
2.00
2.00
4.11
4.02
6.00
f1 (ppm)

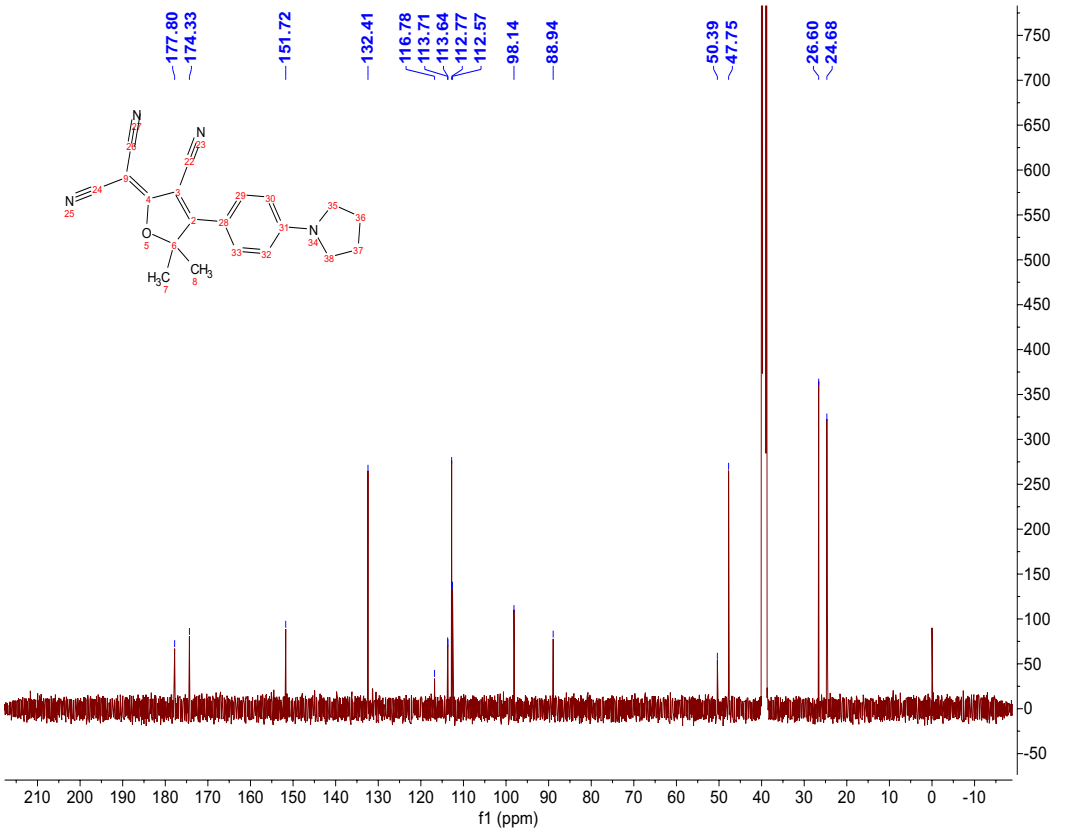
177.80
174.33
151.72
132.41
116.78
113.71
113.64
112.77
112.57
98.14
88.94
50.39
47.75
26.60
24.68
f1 (ppm)

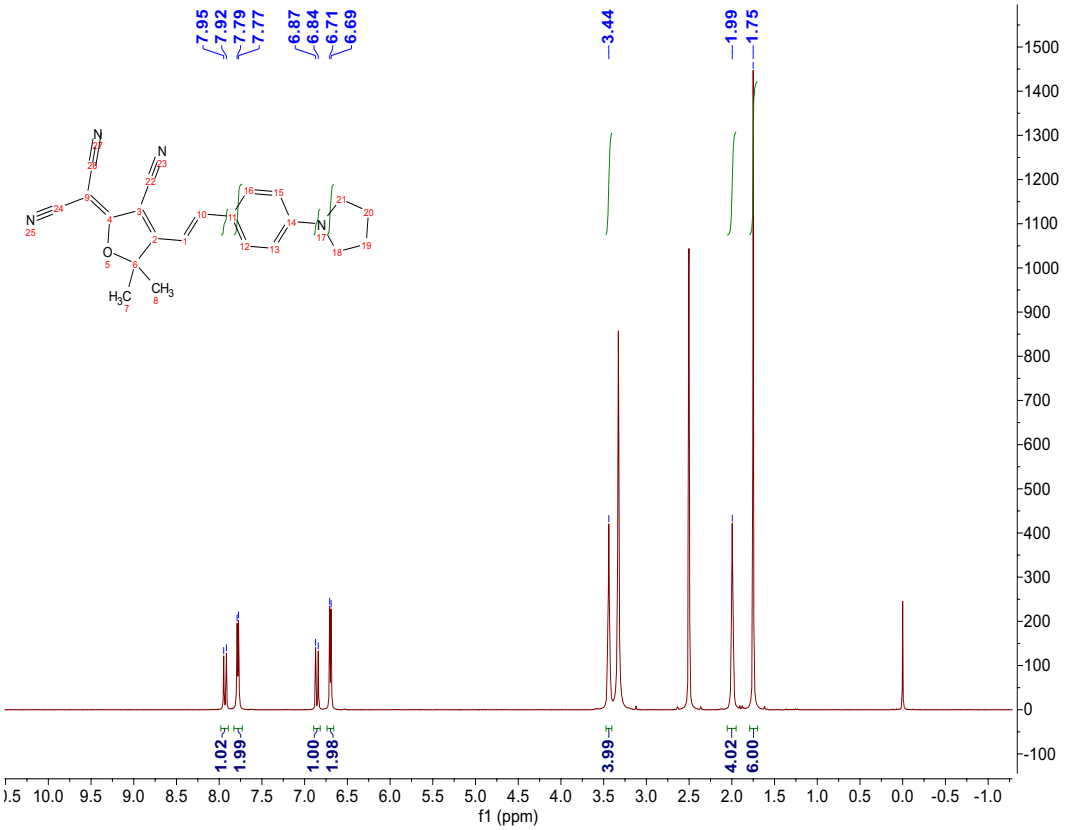
7.95
7.92
7.79
7.77
6.87
6.84
6.71
6.69
3.44
1.99
1.75
1.02
1.99
1.00
1.98
3.99
4.02
6.00
f1 (ppm)

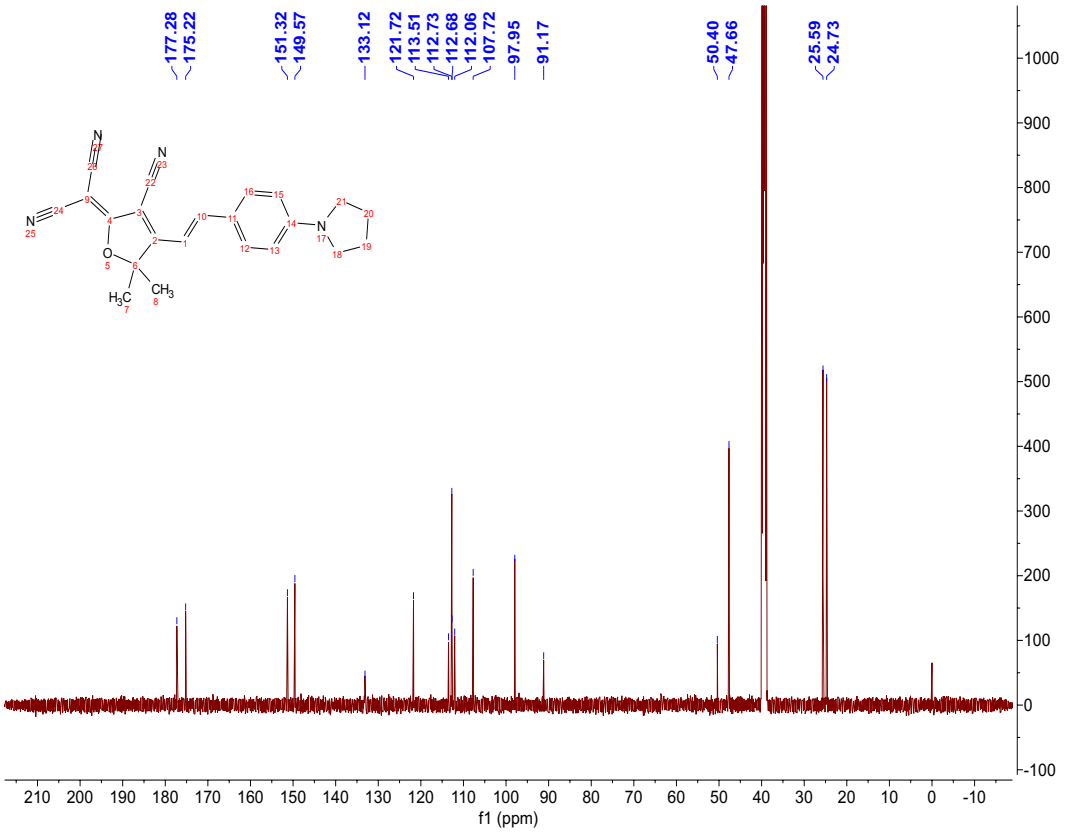
177.28
175.22
151.32
149.57
133.12
121.72
113.51
112.73
112.68
112.06
107.72
97.95
91.17
50.40
47.66
25.59
24.73
f1 (ppm)

5. References

[1] H. J. Yvon, *HORIBA Jobin Yvon Inc, Stanmore, Middlesex, UK* **2012**.
[2] H. Qian, M. E. Cousins, E. H. Horak, A. Wakefield, M. D. Liptak, I. Aprahamian, *Nat. Chem.* **2017**, *9*, 83-87.
[3] N. S. Cheng, *Ind. Eng. Chem. Res.* **2008**, *47*, 3285-3288.
[4] Y. Liu, C. H. Wolstenholme, G. C. Carter, H. Liu, H. Hu, L. S. Grainger, K. Miao, M. Fares, C. A. Hoelzel, H. P. Yennawar, G. Ning, M. Du, L. Bai, X. Li, X. Zhang, *J. Am. Chem. Soc.* **2018**, *140*, 7381-7384.
[5] K. H. Jung, S. F. Kim, Y. Liu, X. Zhang, *ChemBioChem* **2019**, *20*, 1078-1087.
[6] A. Baldridge, J. Kowalik, L. M. Tolbert, *Synthesis* **2010**, *2010*, 2424-2436.
[7] S. Y. Nishimura, S. J. Lord, L. O. Klein, K. A. Willets, M. He, Z. K. Lu, R. J. Twieg, W. E. Moerner, *J. Phys. Chem. B* **2006**, *110*, 8151-8157.
[8] M. Y. Wu, K. Li, C. Y. Li, J. T. Hou, X. Q. Yu, *Chem. Commun.* **2014**, *50*, 183-185.